3-8-2018

α-Catenin-dependent cytoskeletal tension controls Yap activity in the heart.

Alexia Vite

Caimei Zhang

Roslyn Yi

Sabrina Emms

Glenn L. Radice

© 2018. Published by The Company of Biologists Ltd | Development (2018) 145, dev149823. doi:10.1242/dev.149823

STEM CELLS AND REGENERATION

RESEARCH ARTICLE

α-Catenin-dependent cytoskeletal tension controls Yap activity in the heart

Alexia Vite*, Caimei Zhang, Roslyn Yi, Sabrina Emms and Glenn L. Radice‡

ABSTRACT

Shortly after birth, muscle cells of the mammalian heart lose their ability to divide. At the same time, the N-cadherin/catenin cell adhesion complex accumulates at the cell termini, creating a specialized type of cell-cell contact called the intercalated disc (ICD). To investigate the relationship between ICD maturation and proliferation, αE-catenin (*Ctnna1*) and αT-catenin (*Ctnna3*) genes were deleted to generate cardiac-specific α-catenin double knockout (DKO) mice. DKO mice exhibited aberrant N-cadherin expression, mislocalized actomyosin activity and increased cardiomyocyte proliferation that was dependent on Yap activity. To assess effects on tension, cardiomyocytes were cultured on deformable polyacrylamide hydrogels of varying stiffness. When grown on a stiff substrate, DKO cardiomyocytes exhibited increased cell spreading, nuclear Yap and proliferation. A low dose of either a myosin or RhoA inhibitor was sufficient to block Yap accumulation in the nucleus. Finally, activation of RhoA was sufficient to increase nuclear Yap in wild-type cardiomyocytes. These data demonstrate that α-catenins regulate ICD maturation and actomyosin contractility, which, in turn, control Yap subcellular localization, thus providing an explanation for the loss of proliferative capacity in the newborn mammalian heart.

KEY WORDS: αE-catenin, αT-catenin, N-cadherin, Cell adhesion, Intercalated disc, Actomyosin, Mechanotransduction, RhoA

INTRODUCTION

Study of the growth patterns of rodent cardiomyocytes (CMs) during the neonatal period demonstrates that CM number peaks at 4 days of age (Li et al., 1996; Soonpaa et al., 1996). Although CM number remains unchanged thereafter, CM volume and binucleation increase, enlarging the heart via hypertrophic growth. Recent studies have shown that the neonatal murine heart is capable of regeneration following partial surgical resection or myocardial infarction (Porrello et al., 2011, 2013). When the neonatal murine heart undergoes regeneration, the new tissue mostly derives from pre-existing CMs, which is similar to regeneration in adult zebrafish hearts (Jopling et al., 2010; Poss et al., 2002). However, in mice, this regenerative capacity largely disappears in the first week after birth. The cellular and molecular mechanisms responsible for the transient regenerative capacity in the newborn mammalian heart remain poorly understood.

Center for Translational Medicine, Department of Medicine, Thomas Jefferson University, Philadelphia, PA 19107, USA.
*Present address: Department of Medicine, University of Pennsylvania, Philadelphia, PA 19104, USA.

‡Author for correspondence (glenn.radice@jefferson.edu)

G.L.R., 0000-0002-2944-1059

Received 26 January 2017; Accepted 7 February 2018

During the fetal and early postnatal period, the CM elongates, myofibrils align and maturation occurs, resulting in a rod-shaped CM. During this morphological progression, the N-cadherin/catenin cell adhesion complex, which is initially distributed all along the cell borders, becomes restricted to the bipolar ends of the cell, which leads to the formation of a specialized structure called the intercalated disc (ICD) (Angst et al., 1997; Hirschy et al., 2006). Notably, the accumulation of junctional proteins at the ICD coincides with the dramatic decline in CM proliferation in the postnatal period, suggesting that cell adhesion plays a role in myocardial growth control. Moreover, ICD maturation occurs as the heart experiences greater mechanical load when cardiac output increases after birth to support the needs of the newborn organism. Additionally, the local tissue stiffness of the heart remodels in response to changes in the physiological microenvironment during development. According to elastic modulus measurements, normal embryonic cardiac tissue has a Young's modulus of ∼2 kPa, and this increases to 10 kPa in the postnatal myocardium, in relation to myofibril maturation and increasing beating rate (Janmey and Miller, 2011). Increases in tissue stiffness beyond 50 kPa are characteristic of myocardial infarction and are due, at least in part, to excessive fibrosis, which inhibits contraction and promotes stress fiber formation (Berry et al., 2006).

It is well established that assembly and maintenance of the ICD structure is dependent on N-cadherin-mediated adhesion. Cardiac-restricted deletion of either N-cadherin or its binding partners, β-catenin and γ-catenin (plakoglobin), leads to disassembly of the ICD and sudden cardiac death in mice (Kostetskii et al., 2005; Swope et al., 2012). α-Catenin functionally links cadherin and the actin cytoskeleton via its binding to either β-catenin or plakoglobin. Surprisingly, simultaneous ablation of both αE-catenin and αT-catenin in the adult heart does not cause a cardiac phenotype (Li et al., 2015), in contrast to the cardiac-specific β-catenin and plakoglobin double knockout mice that succumb to lethal arrhythmias (Swope et al., 2012). By contrast, depleting α-catenins in the perinatal period prior to ICD formation results in sustained CM proliferation into adult life (Li et al., 2015). These data suggest that α-catenins play an important role in junction remodeling and assembly in the newborn heart. However, after the junction matures after birth, α-catenins are not required to maintain ICD integrity in the unstressed adult myocardium (Li et al., 2015).

Recent studies are beginning to elucidate the molecular mechanism(s) by which α-catenin and its actin-binding partners, particularly vinculin, transduce mechanical force from the cadherin/catenin complex to the cytoskeleton (Hoffman and Yap, 2015; Leckband and de Rooij, 2014; Lecuit, 2010). Changes in actomyosin contractility or tension at the adherens junction alter the conformation of αE-catenin, allowing it to interact with vinculin and thus strengthening the connection between cadherin and the actin cytoskeleton leading to formation of a stable mature junction between epithelial cells (Yao et al., 2014; Yonemura et al., 2010).

Development (2018) 145, dev149823. doi:10.1242/dev.149823

Remodeling of the actomyosin network in response to E-cadherin engagement is responsible for apical constriction during tissue morphogenesis (Martin et al., 2009). Recent studies in epithelial cells demonstrated that changes in cytoskeletal tension regulate Yap activity independently of the Hippo signaling pathway (Aragona et al., 2013; Wada et al., 2011). Mechanical cues that alter the actin cytoskeleton, such as cell spreading, cell geometry and matrix stiffness, have been shown to control Yap subcellular distribution (Dupont et al., 2011). In mammary epithelial cells, perturbing actin organization by knockdown of the F-actin capping/severing proteins cofilin, capZ or gelsolin is sufficient to drive Yap to the nucleus (Aragona et al., 2013). Recent studies have demonstrated the importance of the Hippo pathway and its downstream effector Yap in the regulation of CM proliferation during heart development and following ischemic injury (Heallen et al., 2013, 2011; Lin et al., 2014; von Gise et al., 2012; Xin et al., 2013, 2011). However, the molecular mechanisms that control Yap cellular activity during the transition from hyperplastic to hypertrophic growth phase in the neonatal heart are poorly understood.

Here, we have used complementary *in vivo* and *in vitro* approaches to examine the effect of α-catenin-mediated mechanotransduction on the proliferation of neonatal CMs. In particular, we focused on the relationship between junctional remodeling, actomyosin activity and Yap cellular distribution in the neonatal heart. We show that proper junctional organization of N-cadherin and actomyosin activity during ICD formation is dependent on the cytoskeletal linker proteins αE- and αT-catenin. Using deformable polyacrylamide hydrogels, we show that loss of α-catenins alters cytoskeletal tension, which drives Yap accumulation in the nucleus, causing CM proliferation. Together, our studies reveal a novel α-catenin/Rho/myosin signaling axis that controls cytoskeletal tension and Yap subcellular localization in the neonatal heart.

RESULTS

Yap is required for cardiomyocyte hyperproliferation in α-catenin DKO hearts

To investigate the role of α-catenins in the regulation of cardiomyocyte (CM) proliferation in the postnatal heart, we bred αE-catenin flox (fl), αT-catenin flox and αMHC/Cre mice to generate cardiac-specific αE- and αT-catenin double knockout (DKO) mice (Li et al., 2015). Relevant for these studies, the αMHC/Cre transgene is expressed in the perinatal period prior to maturation of the ICD, which occurs at approximately 2 weeks of age in the mouse, coincident with the switch from hyperplastic to hypertrophic growth. Littermates lacking the Cre transgene (i.e. αE-cat$^{fl/fl}$; αT-cat$^{fl/fl}$) served as wild-type controls. To study the relationship between ICD maturation and Yap, hearts were examined at postnatal day 4 (P4), P7 and P14. Western blot and immunofluorescence analyses showed significant reduction of αE- and αT-catenin proteins in the DKO hearts (Fig. S1), indicating efficient depletion of both α-catenins shortly after birth. Translocation of the transcriptional co-activator Yap to the nucleus is necessary and sufficient to promote CM proliferation *in vivo* (von Gise et al., 2012; Xin et al., 2011). Therefore, we examined postnatal hearts for changes in Yap subcellular distribution during the period of junction remodeling. Hearts were co-stained for Yap and cardiac α-actin. A significant amount of Yap was observed in the cytosol of both wild-type and DKO CMs during this postnatal period (Fig. 1A, Fig. S2). In wild-type hearts, the percentage of nuclear Yap-positive CMs was highest at P4 (56.5%±3.57%) and progressively decreased by P14 (10.15%±0.62%) (Fig. 1B). These data are consistent with the postnatal decline in CM proliferation described previously for rodent hearts (Li et al., 1996; Soonpaa et al., 1996). Loss of α-catenin proteins stimulated nuclear accumulation of endogenous Yap, as demonstrated by an increased percentage of nuclear Yap-positive CMs at P7 (51%±3.67% in DKO versus 34.6%±1.35% in

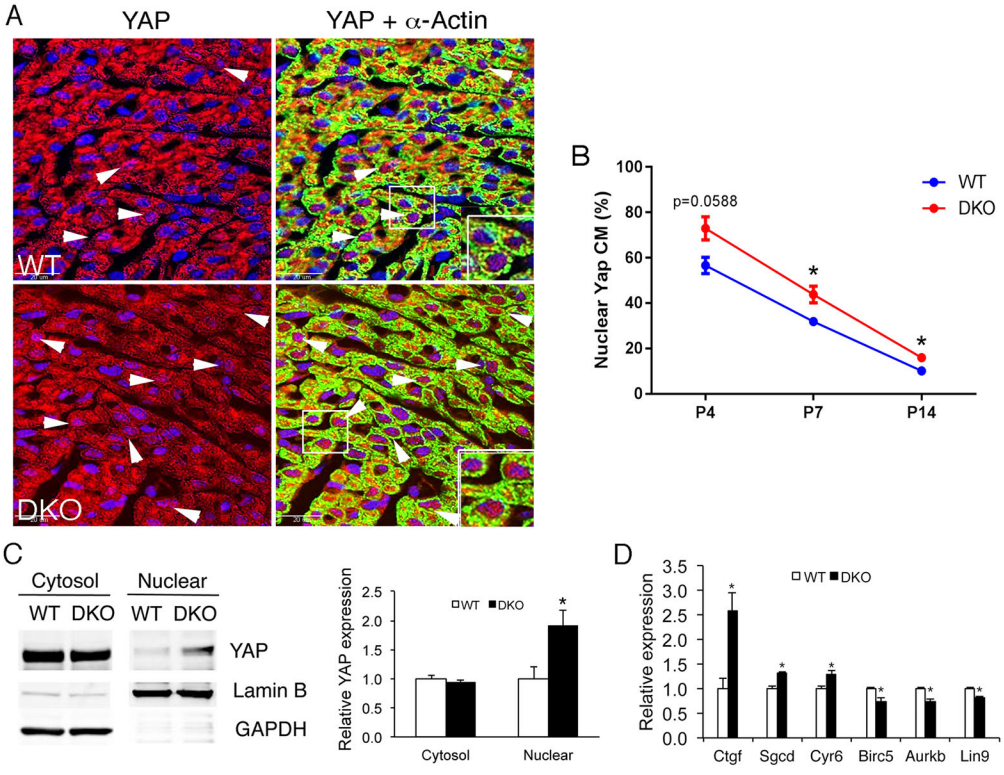

Fig. 1. Yap expression in neonatal hearts. (A) P7 hearts from wild-type and DKO animals were co-immunostained for Yap (red) and α-actin (green). (B) Quantification of nuclear Yap-positive cardiomyocytes in P4, P7 and P14 hearts (n=3). (C) Western blot analysis of cytosol and nuclear fractions from wild-type and DKO hearts. GAPDH and Lamin B serve as controls for enrichment of cytoplasmic and nuclear protein fractions, respectively. Quantification of Yap subcellular fractions (n=3 hearts/genotype). (D) Yap target gene expression assessed by quantitative reverse transcription polymerase chain reaction (qRT-PCR) in wild-type and DKO P7 hearts (n=4 hearts/genotype). *P<0.05 by Student's t-test. Error bars represent s.e.m.

Development (2018) 145, dev149823. doi:10.1242/dev.149823

wild type, $P<0.05$). The Yap signal in the nucleus was also stronger in DKO CMs compared with wild-type CMs (Fig. 1A, insets). Nuclear Yap-positive CMs were also increased in P14 DKO hearts, with P4 trending towards significance ($P=0.058$) (Fig. 1B). Consistent with the immunostaining data, cellular fractionation demonstrated increased Yap in the nucleus of the DKO P7 hearts (Fig. 1C). There was no change in total or phosphorylated Yap (S112) in postnatal DKO hearts (Fig. S3). Next, we examined expression of Yap target genes by quantitative reverse transcription polymerase chain reaction. Yap target genes *Ctgf*, *Cyr61* and *Sgcd* were upregulated, whereas *Birc5*, *Aurkb* and *Lin9* expression was reduced in DKO hearts (Fig. 1D). To ensure proper physiological regulation and homeostasis of cells and organ size, Yap activity is precisely controlled in the cell. To accomplish this, a negative-feedback mechanism has evolved in mammals (Chen et al., 2015; Dai et al., 2015; Moroishi et al., 2015). The downregulation of Yap target genes associated with cell cycle activity suggest a negative-feedback mechanism may be involved in controlling heart size in the absence of α-catenins. Together, these findings indicate that sequestration of Yap in the cytosol is compromised in the DKO hearts, leading to its accumulation in the nucleus and subsequent activation of target genes.

To determine whether Yap was required for the hyperproliferation in DKO hearts, we bred a Yap floxed allele (Schlegelmilch et al., 2011) into the DKO model to generate αMHC/Cre; αE-cat$^{fl/fl}$; αT-cat$^{fl/fl}$; Yap$^{fl/+}$ mice. CMs were isolated from P7 hearts and counted. An increase in total CMs was observed in DKO (4.42×10^5, $n=8$) compared with wild-type (3.19×10^5, $n=20$) P7 hearts (Fig. 2A). Importantly, inactivation of only one Yap allele reduced the total number of CMs to wild-type levels in the DKO; Yap+/− hearts (3.31×10^5, $n=9$). To examine CM proliferation, we analyzed DNA synthesis using 5-ethynyl-2′-deoxyuridine (EdU) incorporation (Fig. 2B,C). The percentage of EdU-positive CMs in DKO hearts (11.73%±0.65%, $n=6$) was about twofold higher than in wild-type (5.52%±0.63%, $n=6$) and DKO; Yap$^{+/-}$ hearts (7.12%±0.64%, $n=6$) at P7. Additionally, proliferation was examined in wild-type, DKO and DKO; Yap$^{+/-}$ CMs isolated from P7 pups. Consistent with the *in vivo* results above, DKO; Yap$^{+/-}$ CMs grown in culture exhibited proliferation rates similar to wild-type CMs (Fig. S4). Collectively, these data demonstrate that Yap activity was responsible for the elevated proliferation rate and increased CM numbers in DKO hearts.

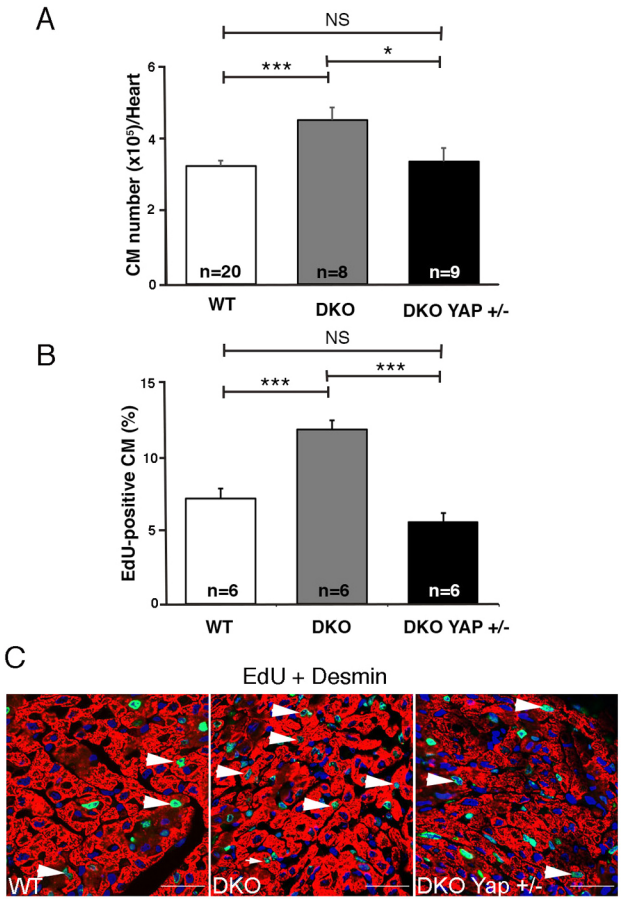

Fig. 2. Yap is required for the increased proliferation in DKO hearts. (A) Cardiomyocyte numbers calculated from wild-type, DKO and DKO Yap$^{+/-}$ P7 hearts. (B) Quantification of EdU-positive cardiomyocytes in P7 hearts from wild-type, DKO and DKO Yap$^{+/-}$ mice, $n=6$ individual hearts/genotype. NS, non-significant, $^*P<0.05$, $^{***}P<0.001$ by Student's *t*-test. Error bars represent s.e.m. (C) EdU (5-ethynyl-2′-deoxyuridine, green) incorporation in P7 hearts from wild-type, DKO and DKO Yap$^{+/-}$ mice. Representative immunofluorescent images of heart sections co-stained for desmin (red) and nuclei highlighted with Draq5 (blue). Arrowheads indicate EdU-positive cardiomyocytes. Scale bar: 20 µm.

Perturbation of ICD maturation and actomyosin activity in postnatal DKO hearts

During postnatal ventricular development, N-cadherin progressively becomes polarized to the bipolar ends of the CM, a prerequisite for ICD assembly. To assess junction maturation in DKO hearts, N-cadherin and β-catenin expression was examined in P4, P7, P14 and 2-month-old hearts. In P4 and P7 wild-type hearts, the junctional proteins were distributed along the lateral membrane and termini before their preferential accumulation to the ICD at P14 (Fig. 3A-C). In P4 DKO hearts, the junctional proteins were localized to the membrane as in wild type. By P7, N-cadherin and β-catenin levels were reduced, especially at the lateral membrane in DKO hearts (Fig. 3B). The organization of the N-cadherin-containing junctional complex was perturbed in DKO hearts. N-cadherin normally exhibits a linear arrangement at the termini beginning around P14 (Fig. 3C, arrows). By contrast, irregular diffuse N-cadherin staining pattern was observed in P14 DKO hearts (Fig. 3C, arrows). In 2-month-old mice, we observed a heterogeneous staining pattern in DKO hearts with N-cadherin localized at the termini in some CMs, whereas other CMs had prominent cytoplasmic staining (Fig. 3D). To further investigate junction remodeling in the DKO model, we used WGA as a membrane marker to compare the relative β-catenin immunosignal intensity between the longitudinal termini (i.e. nascent ICDs) and the lateral membrane of individual CMs (Fig. S5). In wild-type hearts, the percentage of CMs with greater β-catenin at the longitudinal termini progressively increased during postnatal heart development, consistent with maturation of the ICD. By contrast, a lower percentage of CMs with prominent β-catenin at the longitudinal termini was seen in DKO hearts at P14 and 2 months. Interestingly, β-catenin was localized prematurely to the longitudinal termini in newborn DKO hearts (P4 and P7), suggesting a possible compensation mechanism where CMs attempt to transiently re-enforce their junctions when α-catenins are initially depleted. There was no change in either N-cadherin or β-catenin protein levels in postnatal DKO hearts (Fig. S5). Taken together, these data demonstrate that α-catenins are essential for junction remodeling in the postnatal heart.

To determine whether the regulatory effect of α-catenins on Yap activity was associated with a change in cytoskeletal tension, we co-stained P4, P7 and P14 hearts with an antibody recognizing

Development (2018) 145, dev149823. doi:10.1242/dev.149823

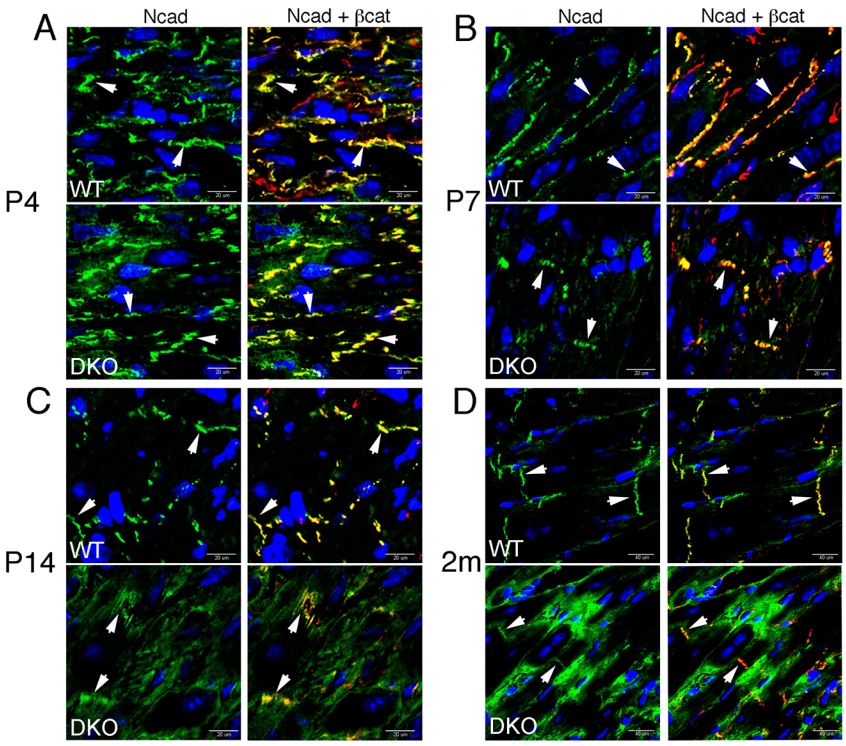

Fig. 3. α-Catenins are required for proper junctional maturation in the postnatal heart. (A-D) Representative immunofluorescent images of heart sections from (A) P4, (B) P7, (C) P14 and (D) 2-month-old wild-type and DKO mice. Sections were co-stained for N-cadherin (green) and β-catenin (red). N-cadherin and β-catenin progressively accumulate at the cell termini (arrowheads). Note the presence of N-cadherin in the cytosol of DKO hearts beginning at P14. DAPI is shown in blue and yellow indicates the colocalization of N-cadherin and β-catenin in the merged image. Arrowheads indicate localization of the cell adhesion molecules at the sarcolemma.

phosphorylated serine 19 of myosin-II regulatory light chain (pMLC), a marker for actomyosin contractility, and N-cadherin. In wild-type hearts, aggregates of pMLC (Fig. 4, hollow arrows) became progressively juxtaposed with N-cadherin (Fig. 4, solid arrows) during junction maturation, P4 to P14. At P4, puncta of pMLC and N-cadherin were in close proximity along the lateral membrane. In comparison with wild type, pMLC aggregates (Fig. 4, hollow arrows) were not as closely aligned with N-cadherin (Fig. 4, solid arrows) in P4 DKO hearts. The proportion of pMLC associated with N-cadherin at the membrane progressively decreased in DKO hearts compared with wild-type hearts at P7 and P14 (Fig. 4B,C). In 2-month-old DKO hearts, we observed a further decrease in both N-cadherin and pMLC at the ICD (Fig. S6).

To further investigate the cellular distribution of actomyosin activity, we cultured CMs isolated from P7 pups and immunostained for pMLC (Fig. 4D). In wild-type CMs, the pMLC signal was primarily localized to regions of cell-cell contact. By contrast, DKO CMs exhibited non-junctional pMLC staining. Next, we isolated adult CMs and stained for pMLC. Actomyosin tension, as depicted by pMLC staining, localized to the termini of wild-type CM (Fig. 4E, arrows). By contrast, pMLC was reduced or absent from the termini in the majority of adult DKO CMs, which correlated with the amount of N-cadherin present at the termini (data not shown). Cross-sectional images derived from 3D reconstruction of confocal images showed that pMLC was localized to the lateral membrane in DKO CM (Fig. 4E). Western analysis was performed on protein lysates from P14 hearts. Interestingly, levels of non-muscle myosin IIb and non-muscle myosin light chain 2, which are components of the actomyosin network, were increased in DKO hearts (Fig. 4F). However, no change in pMLC levels was detected. The difference in myosin IIb levels between wild type and DKO was greater in 2-month-old mice (Fig. S7). Taken together, these data demonstrate that the proper spatial organization of actomyosin activity depends on the mechanosensing proteins αE- and αT-catenin.

DKO CMs exhibit increased proliferation in response to substrate stiffness

Mechanical cues such as cell spreading, cell geometry and matrix stiffness that result in rearrangement of actin cytoskeleton control Yap activity independently of the Hippo kinase cascade (Dupont et al., 2011). The mislocalization of actomyosin contractility to non-junctional sites in DKO CMs, as determined by pMLC staining pattern, implies a shift in cytoskeletal tension away from the ICD in favor of intracellular tension. To determine whether the redistribution of actomyosin activity affected the ability of DKO CMs to sense extracellular stiffness, we adapted the use of deformable polyacrylamide hydrogels coated with fibronectin (PA-FN). A range of elastic conditions corresponding to physiological (10 kPa), intermediate (25 kPa) and pathological stiffness (50 kPa) was used. After 4 days, the cultures were subconfluent, containing neonatal CMs with varying degrees of cell-cell interactions as well as single cells (Fig. 5D). CMs grown on PA-FN hydrogels were co-stained for Yap and cardiac α-actin. On stiff substratum, the extent of cell spreading generally correlates with the amount of intracellular tension generated by the cell, i.e. cells exert greater force on stiffer surfaces, thereby increasing their spread area. As described previously (Chopra et al., 2011; Engler et al., 2008; Jacot et al., 2008), CMs cultured on PA-FN hydrogels corresponding to physiological stiffness (i.e. 10 kPa) developed a rod-shaped morphology over time with more striations compared with cells grown on stiffer substrates (25 kPa, 50 kPa) (Fig. 5A). Notably, CM area was increased (+17%, n=7, P<0.05) in DKO cultures grown under stiffness conditions associated with scar tissue post-MI (i.e. 50 kPa), whereas no difference in area was observed between wild type and DKO on the more compliant substrates (10 kPa, 25 kPa) (Fig. 5B).

Next, we examined the relationship between cytoskeletal tension generated by the different substrate stiffnesses and Yap subcellular localization. Nuclear YAP was increased in DKO CMs compared with wild-type CMs grown on 50 kPa (Fig. 5C). By contrast, no

Development (2018) 145, dev149823. doi:10.1242/dev.149823

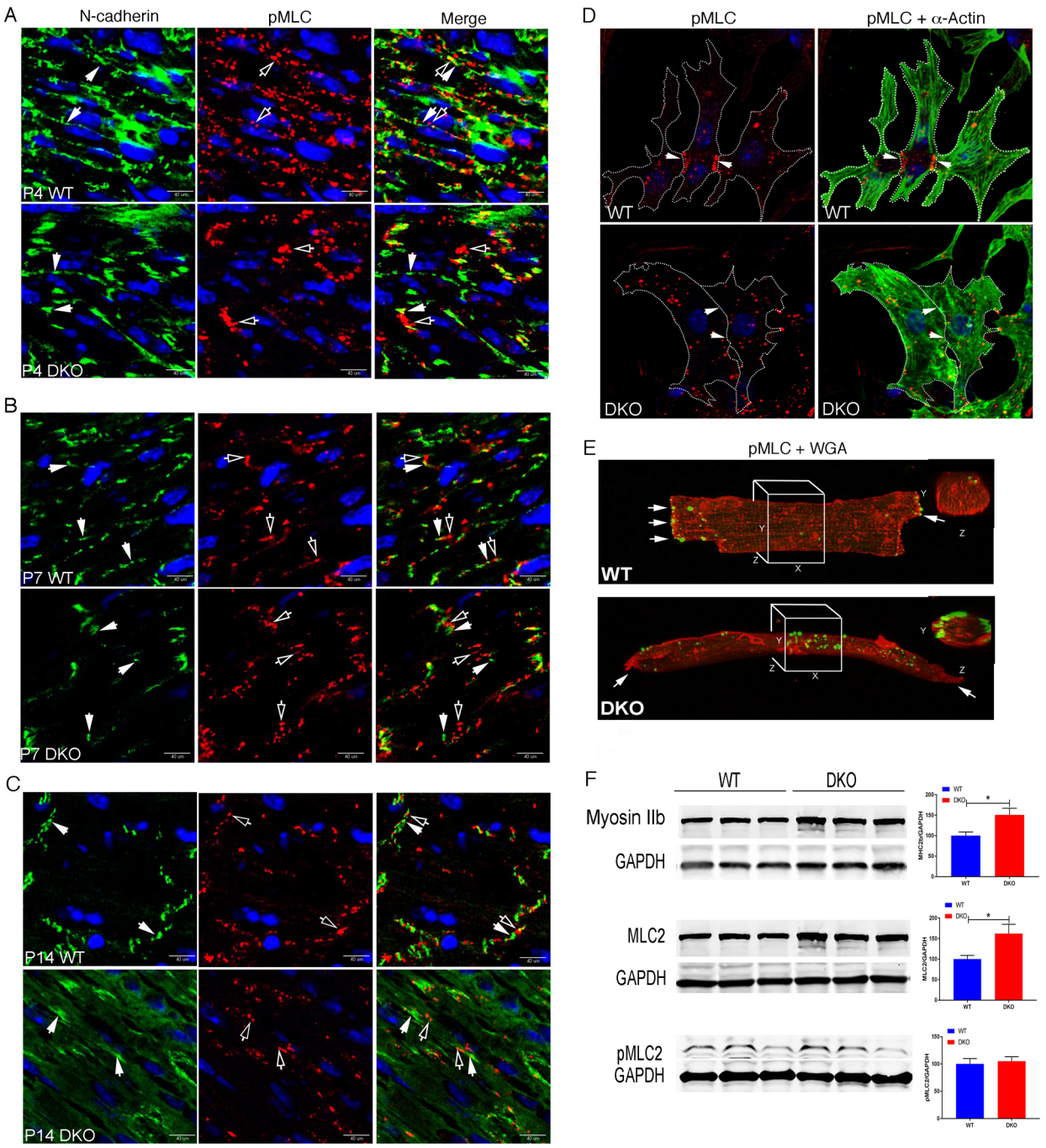

Fig. 4. Mislocalization of actomyosin activity in α-catenin-deficient cardiomyocytes. (A-D) Representative immunofluorescent images of heart sections from P4 (A), P7 (B) and P14 (C) wild-type and DKO mice. Sections were co-stained for N-cadherin (green, solid arrowheads) and pMLC (red, hollow arrowheads). (D) Cardiomyocytes were isolated from wild-type and DKO neonatal P7 hearts, and cultured for 4 days to allow junction formation. Cells were co-stained for pMLC (red, arrowheads) and α-actin (green). A stippled line outlines cardiomyocyte borders. (E) Isolated cardiomyocytes from 2-month-old wild-type and DKO hearts were immunostained for pMLC (green) and WGA (red). A three-dimensional reconstruction was generated from a series of confocal optical sections. Cross-sectional images (inset) represent the boxed area shown. Arrows indicate the longitudinal termini of the adult cardiomyocyte. (F) Western blot analysis and quantification of myosin IIb, MLC and pMLC expression in whole heart lysates from P14 mice. **P*<0.05 by Student's *t*-test. Error bars represent s.e.m.

change in nuclear Yap was observed in CMs grown on 10 kPa and 25 kPa PA-FN hydrogels. Finally, we confirmed that the presence of Yap in the nucleus correlated with the rate of proliferation. To examine CM proliferation, we analyzed DNA synthesis in CMs using 5-bromo-2′-deoxyuridine (BrdU) incorporation. Indeed, the percentage of BrdU-positive CMs was greater in DKO CMs compared with wild-type CMs when cultured on stiffer PA-FN hydrogels (Fig. 5D,E). Interestingly, the difference in spreading and nuclear Yap observed on 50 kPa was not seen when wild-type and DKO CMs were grown on stiffer substrate (i.e. 100 kPa, data not shown), suggesting that loss of α-catenins affects mechanotransduction over a limited range of stiffness, i.e. corresponding to the pathological stiffness of heart tissue post-MI (Berry et al., 2006). Taken together, these findings demonstrate that

Development (2018) 145, dev149823. doi:10.1242/dev.149823

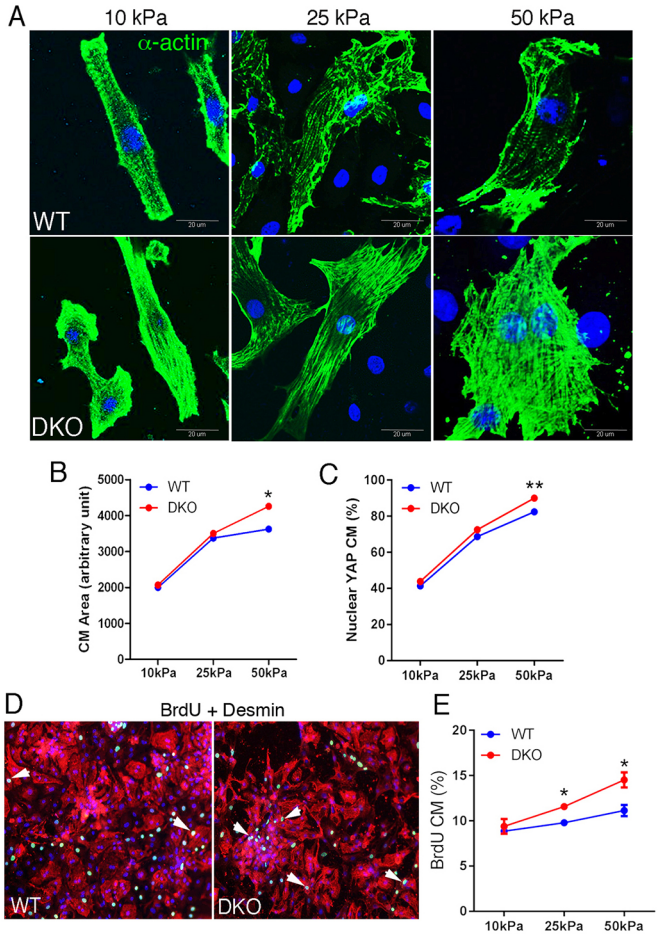

Fig. 5. α-Catenin DKO cardiomyocytes exhibit increase proliferation on stiff ECM. (A) Representative images of neonatal cardiomyocytes cultured on different PA-FN stiffness for 4 days and stained for α-actin (green) and DAPI (blue). (B,C) Quantification of (B) cell area and (C) nuclear Yap in cardiomyocytes grown on different stiffnesses. (D) Representative images of BrdU (5-bromo-2′-deoxyuridine, green) incorporation (arrowheads) in cultured neonatal cardiomyocytes (desmin, red). Cells were co-stained for desmin (red). (E) Quantification of BrdU-positive cardiomyocytes cultured on different stiffnesses (*n*=3 experiments, *n*=minimum 100 cells/experiment). **P*<0.05, ***P*>0.01 by Student's *t*-test. Error bars represent s.e.m.

loss of α-catenins increases intracellular forces in response to pathological stiffness and, in turn, promotes Yap activity and CM proliferation.

Myosin II contractility mediates the affects of α-catenin inhibition on Yap

To determine whether actomyosin activity was required for the hyperproliferative phenotype, we treated DKO CMs with different inhibitors of actomyosin contractility. Initially, we analyzed DKO CMs grown on nondeformable substrata, i.e. standard glass coverslips. Yap distribution was examined in DKO CMs after treatment with the contractility inhibitors, blebbistatin, ML-7 and Y27632, which inhibit myosin-II ATPase, myosin light-chain kinase and Rho kinase, respectively. Blocking actomyosin contractility with any of these inhibitors disrupted myofibril organization and caused Yap to exit the nucleus (Fig. S8). The increased cell area or spreading observed in DKO CMs cultured on 50 kPa (Fig. 5B) suggests that DKO CMs exert greater force on stiff substrata, which is opposed by increased tension in the cell. Therefore, we hypothesized that an increase in tension would render DKO CMs more sensitive than wild-type CMs to the myosin inhibitor blebbistatin. To further address the relationship between myosin II contractility and Yap localization, we performed a blebbistatin dose-response experiment (1, 5 and 10 µM) with CMs grown on 50 kPa PA-FN hydrogels. Representative images of the effects of blebbistatin on CM spreading are shown (Fig. 6A). A low dose of blebbistatin (1 µM) was sufficient to significantly decrease CM area in DKO cultures, whereas a 10-fold higher dose was necessary to have a similar effect on CM area in wild-type cultures. Importantly, the change in CM area was accompanied by a similarly striking decrease in nuclear Yap in DKO CMs compared with wild-type CMs. These findings demonstrate that non-muscle myosin-II contractility is required for the increased nuclear Yap in DKO CMs.

RhoA is required for changes in cytoskeletal tension and Yap nuclear localization

RhoA is a primary upstream regulator of myosin II contractility; therefore, we examined Rho GTPase activity in freshly isolated P7 heart tissue using G-LISA. Rho-GTP levels were increased in DKO hearts (*n*=9) compared with the wild-type hearts (*n*=9) (Fig. 7A), consistent with an increase in actomyosin activity and CM area in DKO CMs grown on stiff PA-FN hydrogels (Fig. 5A). To test whether elevated RhoA activity is required for the increased actomyosin contractility and Yap activity in DKO hearts, CMs were cultured on 50 kPa PA-FN hydrogels and treated with the Rho inhibitor CT04 (Fig. 7). Representative images of the effects of CT04 on CM spreading and myofibril organization are shown (Fig. 7B). Compared with wild type, DKO CMs displayed increased sensitivity to the Rho inhibitor, as illustrated by decreased spreading at the lowest dose of CT04 (0.25 µg/ml) (Fig. 7C). By contrast, CM area was not affected in wild-type cultures treated with the same dose of CT04. Similar to blebbistatin treatment, the decrease in DKO CM area induced by low dose CT04 treatment resulted in a striking decrease in the percentage of nuclear Yap-positive CMs in the DKO cultures (Fig. 7D). In wild type, a higher dose of CT04 was required to have a similar effect on Yap nuclear localization, as observed in DKO cultures.

Next, we tested whether activation of RhoA was sufficient to induce translocation of Yap to the nucleus. Endogenous RhoA activity (i.e. RhoA-GTP) is lower on soft substrate compared with stiff (Paszek et al., 2005); therefore, the effects of the Rho activator CN03 were examined in CMs cultured on compliant 12 kPa PA-FN hydrogels (Fig. 8). Representative images of the effects of CN03 on CM morphology after a 3 h treatment are shown (Fig. 8A). Rho activation caused increased CM spreading accompanied by increased nuclear Yap on compliant substrata (Fig. 8B,C). Interestingly, the response to Rho activation was similar between wild-type and DKO CMs under these experimental conditions (data not shown), consistent with the idea that cellular tension, corroborated by extent of cell spreading, is similar between wild-type and DKO CMs when cultured on compliant substrate (Fig. 5B). Together, these data demonstrate that activation of Rho is necessary and sufficient to increase cytoskeletal tension, resulting in Yap accumulation in the nucleus of neonatal CMs.

DISCUSSION

In this study, we show a significant decline in the percentage of nuclear Yap-positive CMs between P4 and P14, coincident with the precipitous drop in CM proliferation during this period. We found that loss of α-catenins resulted in Yap accumulation in the nucleus and upregulation of a subset of Yap target genes consistent with a

Development (2018) 145, dev149823. doi:10.1242/dev.149823

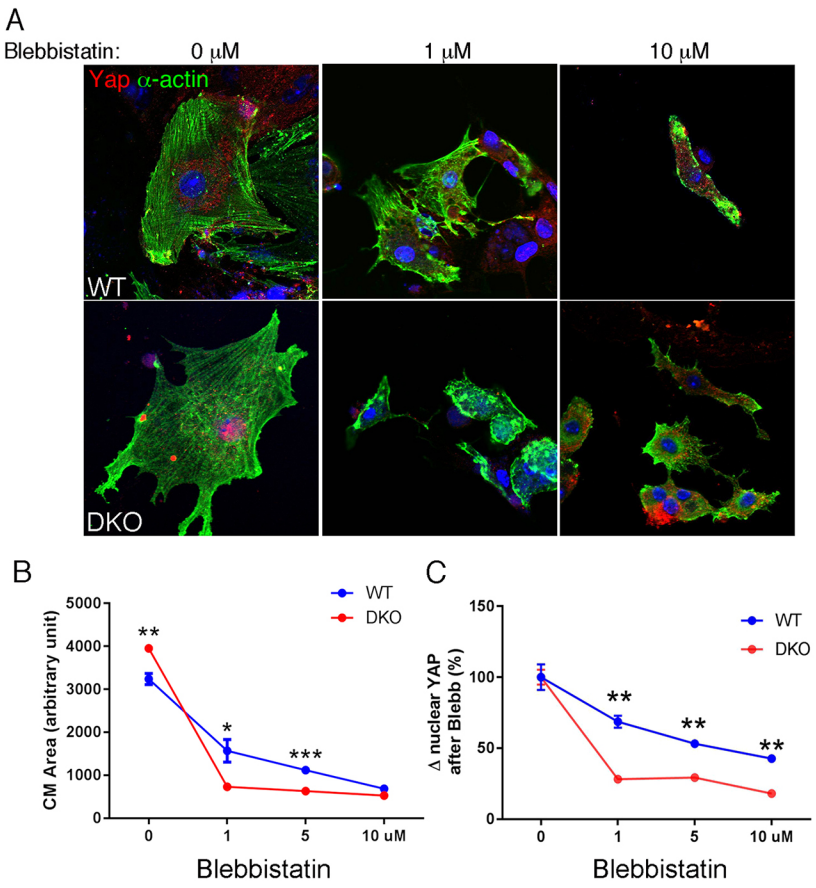

Fig. 6. Loss of α-catenins leads to increased sensitivity to blebbistatin. (A) Representative images of cardiomyocytes cultured on PA-FN hydrogels (50 kPa) for 4 days and treated for 3 h with increasing doses of blebbistatin. The cells were co-stained for Yap (red) and α-actin (green). (B,C) Quantification of (B) cell area and (C) percent change in nuclear Yap after blebbistatin treatment (*n*=3 experiments, *n*=minimum 100 cells/experiment). Note the significant decline in cell area and nuclear Yap after treating DKO cardiomyocytes with a low dose (1 μM) of blebbistatin. **P*<0.05, ***P*<0.01, ****P*<0.001 by Student's *t*-test. Error bars represent s.e.m.

role for Yap in the proliferative phenotype in the α-catenin DKO hearts. Indeed, this was the case because introduction of a Yap floxed allele into the DKO background was sufficient to restore CM numbers and proliferation rate to wild-type levels. Consistent with our results, expression of constitutively active Yap in CMs beginning at P5 has been shown to be sufficient to drive proliferation in the mouse heart (von Gise et al., 2012). Taken together, we conclude that increased Yap activity is responsible for the sustained CM proliferation in DKO hearts, which normally exit the cell cycle during the first week after birth.

The functional interdependence between E-cadherin and actomyosin contractility in the establishment of adherens junctions in epithelial cells is well documented (Miyake et al., 2006; Rauzi et al., 2010; Shewan et al., 2005; Smutny et al., 2010). However, little is known regarding the functional relationship between N-cadherin and actomyosin-generated tension in cardiac homeostasis. Heart muscle contains both muscle-specific myosins and non-muscle myosins (NM), the latter of which is normally downregulated in adult myocardium (Ma and Adelstein, 2014). NMIIB, one of the three NM isoforms, is required for CM cytokinesis, and its expression is reduced after birth as CMs differentiate and exit the cell cycle (Takeda et al., 2003). Here, we show that actomyosin activity, as depicted by pMLC immunostaining, is preferentially located at the ICD in close proximity to N-cadherin. By contrast, pMLC is no longer present at cell-cell contacts but rather it is found at nonjunctional sites in DKO CMs. The redistribution of actomyosin contractility indicates a shift in intercellular or polarized tension away from the ICD in favor of intracellular tension. Interestingly, the reorganization of actomyosin activity was accompanied by an increase in NMIIB, consistent with its role in CM cytokinesis and the increased proliferation in DKO hearts. In support of our findings, it has recently been shown that disruption of N-cadherin junctions during lens fiber cell morphogenesis leads to increased actomyosin activity in mice (Logan et al., 2017).

To understand how α-catenin-deficient CMs sense and respond to their microenvironment, we used deformable polyacrylamide (PA) hydrogels of varying stiffnesses. Consistent with previous studies (Chopra et al., 2011; Engler et al., 2008; Jacot et al., 2008), regardless of genotype, neonatal CMs cultured on substrate corresponding to physiological stiffness (10 kPa) led to CM elongation and myofibril alignment compared with CMs on stiff substrate (50 kPa). As predicted, CM spread area was increased in both wild-type and DKO CMs when grown on stiff (50 kPa) compared with compliant (10 kPa) substrate. Importantly, DKO CMs showed a greater increase in cell spread area compared with wild-type CMs when grown on stiff substrate, consistent with an increase in cellular tension generated by the actomyosin network. The greater CM area was accompanied by increased nuclear Yap and elevated proliferation in DKO CMs. By contrast, there was no difference in CM area, Yap or proliferation when wild-type and DKO CMs were grown on compliant PA hydrogels, supporting the idea that the proliferative phenotype is driven by tension generated in response to stiff substrata. Interestingly, the difference between wild type and DKO with respect to CM spread area and proliferation disappeared as the stiffness reached 100 kPa (data not shown). Our data indicate that DKO CMs experience mechanotransduction over a range of stiffnesses that parallels that reported for post-MI myocardium (50–90 kPa) (Berry et al., 2006). Moreover, DKO CMs exhibit increased sensitivity to myosin inhibitors that resulted in dramatic changes in CM spread area, specifically when cells were

Development (2018) 145, dev149823. doi:10.1242/dev.149823

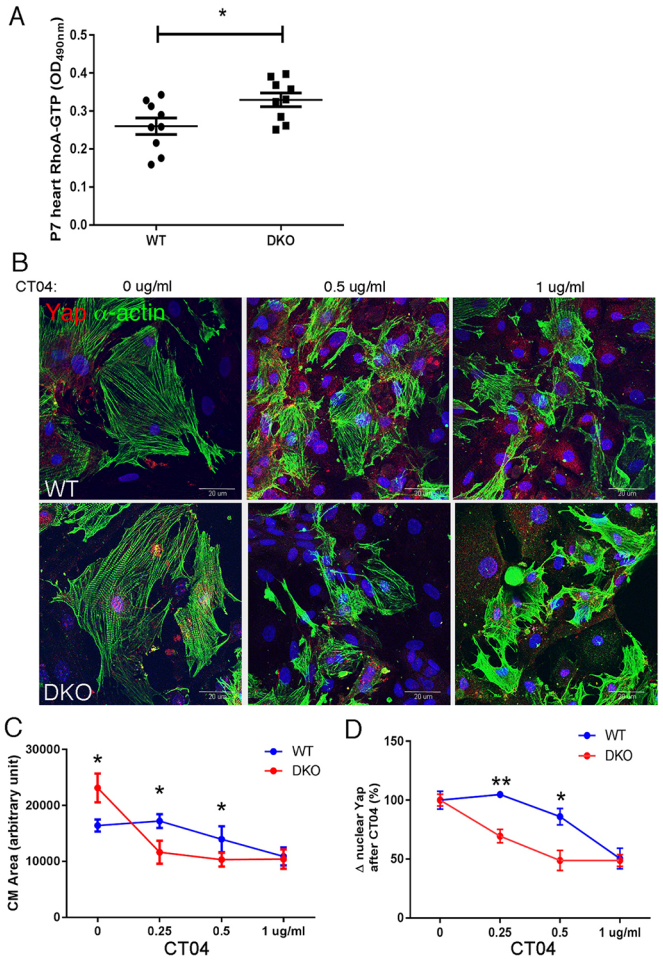

Fig. 7. Rho is required for nuclear Yap accumulation in α-catenin DKO cardiomyocytes. (A) Quantification of Rho activity in freshly isolated hearts from wild-type and DKO P7 mice (*n*=9) by G-LISA. (B) Representative images of cardiomyocytes cultured on PA-FN hydrogels (50 kPa) for 4 days and treated for 3 h with increasing doses of Rho inhibitor (CT04). The cells were co-stained for Yap (red) and α-actin (green). (C,D) Quantification of (C) cell area and (D) percent change in nuclear Yap after CT04 treatment (*n*=4 experiments, *n*=minimum 100 cells/experiment). There is a significant decline in cell area and nuclear Yap after treating DKO cardiomyocytes with a low dose (0.25 µg/ml) of CT04. **P*<0.05, ***P*<0.01 by Student's *t*-test. Error bars represent s.e.m.

grown on stiff substrate (i.e. 50 kPa). Importantly, relieving tension with myosin inhibitors caused Yap to exit the nucleus. Inhibition of Rho activity in CMs cultured on 50 kPa PA-FN hydrogels induced a dose-dependent decrease in CM area accompanied by Yap exit from the nucleus. Conversely, we show that activation of Rho in wild-type CMs grown on compliant PA-FN hydrogels (i.e. 12 kPa) led to increase in cell spreading and in nuclear Yap. Evidence from earlier transgenic mouse studies supports a role for Rho GTPase activity in myocardial proliferation (Wei et al., 2002). In this study, early cardiac-specific expression of the Rho inhibitor Rho GDIα disrupted cardiac morphogenesis and reduced CM proliferation, resulting in embryonic lethality. Further studies are necessary to determine whether altering cellular tension in the postnatal heart and in the adult heart following ischemic injury is sufficient to stimulate CM proliferation.

In a recent study, Yahalom-Ronen et al. investigated the effects of substrate stiffness on CM proliferation and the authors reached a seemingly different conclusion from ours (Yahalom-Ronen et al., 2015). They reported that culture of neonatal CMs on 'compliant' (20 kPa) polydimethylsiloxane (PDMS) substrate promoted de-differentiation and cell cycle re-entry compared with CMs grown on rigid substrate (2000 kPa). The discrepancy between their results and the present study may be explained, at least in part, by differences in experimental design. Whereas we cultured CMs on polyacrylamide substrates with a stiffness range corresponding to healthy postnatal heart tissue (10 kPa) to fibrotic diseased myocardium (50 kPa), Yahalom-Ronen et al. cultured neonatal CMs on a wider range of stiffness corresponding to embryonic myocardium (5 kPa), adult myocardium (20 kPa) and an extremely rigid substrate (2000 kPa) that has no comparable physiological state. Importantly, their proliferation data for CMs cultured on physiologically relevant stiffnesses (5 and 20 kPa) actually supports our findings, i.e. increased stiffness drives CM proliferation, and is consistent with previous studies with various cell types (Klein et al., 2009; Mih et al., 2011; Wang et al., 2000). In response to matrix stiffening, cells increase actomyosin contractility, which is required for the increase in proliferation observed on stiff substrate. Yahalom-Ronen et al. reported that inhibition of actomyosin contractility with blebbistatin resulted in increased CM proliferation, data that are inconsistent with our blebbistatin results showing that nuclear Yap is dependent on actomyosin activity, and as previously described (Das et al., 2016; Dupont et al., 2011). Notably, Yahalom-Ronen et al. observed the stimulatory effect on rigid substrate, while blebbistatin has been shown to stimulate proliferation when cells are cultured specifically on soft substrate (<1 kPa) (Mih et al., 2012, 2011). Future studies using similar experimental conditions will be necessary to reconcile the different findings.

Recent evidence suggests that Yap regulates cardiac repair through multiple mechanisms. Interestingly, Yap was shown to directly regulate genes encoding proteins that control cytoskeletal dynamics, suggesting a positive-feedback loop may exist that maintains nuclear Yap localization (Morikawa et al., 2015). This study identified *αT-catenin* (*Ctnna3*) as a Yap target gene, but not *αE-catenin* (*Ctnna1*), suggesting a unique role for αT-catenin in CM cytoskeletal remodeling. These two α-catenin isoforms have overlapping functions; however, the recently evolved αT-catenin has acquired molecular properties distinct from αE-catenin. For example, αT-catenin contains a plakophilin (PKP)-binding site that is not present in αE-catenin (Goossens et al., 2007). The ability of αT-catenin to interact with PKP-2 promotes mixing of classical and desmosomal cadherin adhesion complexes to create a specialized junctional complex in the heart referred to as the area composita (Franke et al., 2006). Additionally, αT-catenin binds to both F-actin and β-catenin simultaneously in the absence of tension, whereas αE-catenin requires tension to link cadherin to the actin cytoskeleton (Wickline et al., 2016). Further studies are warranted to understand the effects of Yap on actin dynamics, which play a crucial role in junctional remodeling during cardiac development and following ischemic injury.

Cells sense and transduce mechanical signals through a combination of cell-cell adhesions and cell-ECM adhesions. In the heart, CMs modulate local tissue stiffness (micro-elasticity) to adapt to mechanical load and to remodel their cytoskeleton network in response to extracellular rigidity (Majkut et al., 2014). Integrins cluster at focal adhesions and, like cadherins, link to the actin cytoskeleton. Fibronectin, a major ECM protein, and its receptor, integrin α5, are downregulated after birth as the N-cadherin adhesion complex accumulates at the ICD, suggesting cooperation between the two adhesion systems as the newborn heart responds to the increased mechanical load. Here, we show that DKO CMs exhibit increased proliferation when cultured specifically on a stiff

Development (2018) 145, dev149823. doi:10.1242/dev.149823

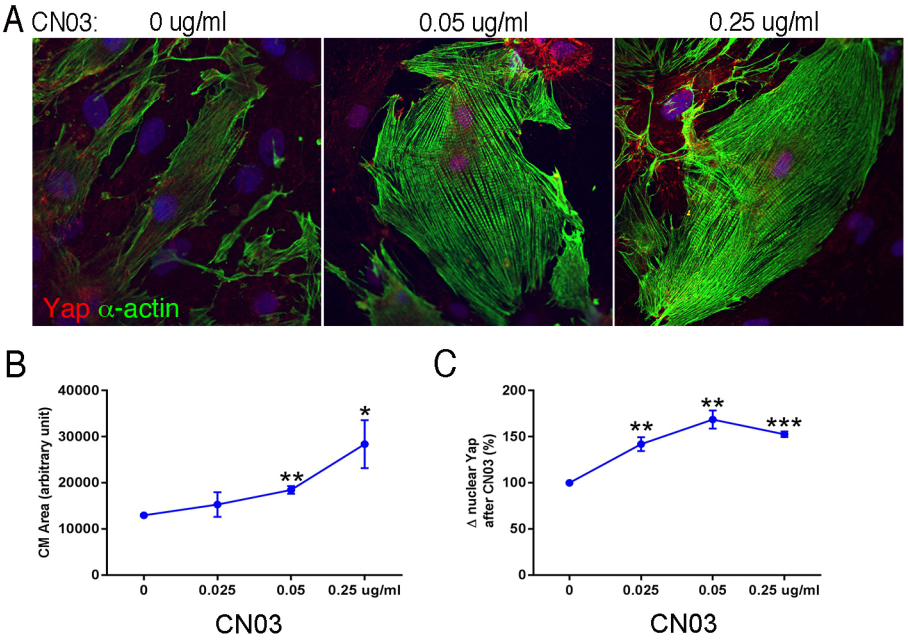

Fig. 8. Activation of Rho is sufficient to drive Yap to the nucleus in wild-type cardiomyocytes. (A) Representative images of cardiomyocytes cultured on PA-FN hydrogels (12 kPa) for 4 days and treated for 3 h with increasing dose of Rho activator (CN03). The cells were co-stained for Yap (red) and α-actin (green). (B,C) Quantification of (B) cell area and (C) percent change in nuclear Yap after CT04 treatment (n=4 experiments, n, minimum 100 cells/experiment). *P<0.05, **P<0.01, ***P<0.001 by Student's t-test. Error bars represent s.e.m.

substrate; hence, it will be of interest to determine whether altered CM-derived tension leads to enhanced matrix assembly and stiffness in DKO hearts.

Here, we show that loss of α-catenins affects junctional remodeling and Yap subcellular distribution in the postnatal heart. We have previously shown that deletion of α-catenins in the unstressed adult heart after establishment of the ICD did not affect Yap localization and CM proliferation, suggesting that the state of maturation of the junction is important for the proliferative phenotype. Following ischemic injury, the remaining viable myocardium surrounding the infarct experiences junction remodeling. CMs located at the border zone of infarcted rat hearts exhibit ICD remodeling associated with perturbed N-cadherin expression (Matsushita et al., 1999). Following MI, the lost heart muscle is replaced by scar tissue. The deposition of ECM at the injury site increases stiffness of the heart tissue (>50 kPa). Our recent work showed that when α-catenins are inactivated in adult hearts following MI, nuclear Yap increases, CM proliferation increases and cardiac function improves (Li et al., 2015). Together, these data suggest that junctional remodeling and the cardiac microenvironment (i.e. stiffness due to fibrosis) synergistically regulate Yap subcellular distribution in the MI setting.

In conclusion, the ability of α-catenins to regulate actomyosin-generated tension and its effects on Yap subcellular distribution have important implications for understanding the loss of proliferative capacity in the heart shortly after birth. The pro-proliferative relationship between junction dynamics, ECM stiffness and Yap nuclear translocation, which we observed in neonatal CMs, may also occur in the injury setting where CMs experience junction remodeling in the context of a stiff ECM in the infarcted myocardium. A key avenue for future investigations will be to explore whether altering actomyosin contractility or tension *in vivo* is sufficient to stimulate CM proliferation.

MATERIALS AND METHODS

Generation of cardiac-specific αE- and αT-catenin double knockout (DKO) mice

αMHC/Cre; αE-catenin$^{fl/fl}$; αT-catenin$^{fl/fl}$ (DKO) animals were generated as previously described (Li et al., 2015). Yap floxed mice, kindly provided by Dr Fernando Carmago (Boston Children's Hospital), were bred into the DKO background. The mice were maintained on a mixed 129Sv-C57BL/6J genetic background. All animal experiments were performed in accordance with the guidelines of the IACUC of Thomas Jefferson University.

Immunofluorescent staining

Paraffin wax- and OCT-embedded tissues were used for immunofluorescence staining. Paraffin sections (5 µm) were deparaffinized, rehydrated and subjected to heat-induced epitope retrieval. OCT sections (5 µm) were fixed in 4% paraformaldehyde (PFA) followed by 100% methanol for 10 min at −20°C. For primary neonatal cardiomyocyte cultures, cells were directly fixed for 10 min in 4% PFA at room temperature and permeabilized in 0.1% Triton X-100.

Specimens were blocked in T-BSA (0.01% Triton X-100 in 5% BSA) and incubated overnight at 4°C with primary antibodies: YAP (1:200, 4912, Cell Signaling Technology), cardiac α-Actin (1:200, cultured cells; 1:100, tissue, A9357, Sigma), Desmin (1:200, D828-1, Sigma), BrdU (BrdU Labeling and Detection Kit I 11296736001, Roche), N-cadherin (1:200, 610921, BD Bioscience), β-catenin (1:200, 712700, Life Technologies), phospho-MLC2 (1:200, 3674, Cell Signaling), αE-catenin (1:50, 711200, Life Technologies) and αT-catenin (1:100, 13974-1-AP, Proteintech). After washing in PBS, cells were incubated with the secondary antibody (Alexa Fluor 555 goat anti-rabbit or donkey anti-mouse IgG, Alexa Fluor 488 goat anti-mouse or 488 rabbit anti-goat IgG and Alexa Fluor 647 donkey anti-rabbit IgG; Life Technologies) for 1 h. Finally, specimens were washed in PBS and mounted with ProLong Gold Antifade Reagent containing DAPI (Life Technologies). Images were collected using a Zeiss LSM 510 META Confocal Microscope System. Images were analyzed using IMAGEJ 1.43 software.

For isolated adult cardiomyocytes, cells were fixed in 4% PFA at room temperature for 10 min then directly stained with Wheat Germ Agglutinin (WGA) and Texas Red-X conjugate (W21405, Life Technologies) at 10 µg/ml for 30 min. The cells were then permeabilized in 0.1% Triton X-100 before being stained for 2 h at room temperature with phospho-MLC2 (1:200, 3674, Cell Signaling) primary antibody then with Alexa Fluor 488 goat anti-rabbit for 1 h. Finally, cells were washed in PBS and mounted into ProLong Gold Antifade Reagent with DAPI (Life Technologies). A series of optical sections were collected at 0.2 µm intervals, moving progressively through the cell using a Nikon A1R^{+} confocal microscope. For 3D-reconstruction, images were analyzed using IMAGEJ 1.43 software.

Cardiomyocyte isolation and culture conditions

Cardiomyocytes were isolated from wild-type and DKO postnatal day 7 (P7) mice using the Mice/Rat neonatal heart dissociation kit (130-098-373,

Development (2018) 145, dev149823. doi:10.1242/dev.149823

Miltenyi Biotec) and the gentleMACS Octo Dissociator (130-096-427, Miltenyi Biotec), according to the manufacturer's protocol. Briefly, ventricles were isolated and incubated in the enzyme Mix in C-tubes using the program 37C_mr_NHDK_1. After digestion, the cell suspension was resuspended in 7.5 ml of 10% horse serum medium [10% horse serum, 1% penicillin/streptomycin in DMEM, low glucose, pyruvate, HEPES (12320032, Life Technologies)]. Cells were filtered in a MACS SmartStrainer of 70 µm (130-098-462, Miltenyi Biotec). After rinsing, the cells were centrifuged for 5 min at 600 ***g*** and the pellet was resuspended in 10 ml of medium. To enrich for cardiomyocytes, cells were preplated for 2 h at 37°C. Non-adherent cells were removed and plated on fibronectin-coated glass coverslips or polyacrylamide hydrogels (ITMAT Biomechanics Core, University of Pennsylvania, Philadelphia, PA, USA or Matrigen) and cultured in 10% horse serum medium. After 16 h, the cells were washed and cultured for 3 days in 5% horse serum medium. Adult cardiomyocytes were isolated as previously described (Li et al., 2015).

Monitoring DNA synthesis with EdU and BrdU labeling

For assessing cardiomyocyte proliferation in heart tissue, mice were injected with EdU (20 mg/kg) at P3, P5 and P7. Two hours after the last injection, the hearts was removed and fixed in PFA. DNA synthesis was revealed with Click-iT EdU Alexa Fluor 488 Imaging Kit (C10337, Life Technologies) following the manufacturer's instructions.

For assessing cardiomyocyte proliferation *in vitro*, cultures were incubated with 10 µM BrdU (BrdU Labeling and Detection Kit I,11296736001, Roche) for 24 h before fixation. Cells were double-stained using anti-BrdU and Desmin (1:200, D828-1, Sigma) antibodies and assessed by indirect immmunofluorescence.

Western blot analysis

Hearts tissue were homogenized in a modified RIPA buffer [50 mM Tris-HCl (pH 7.5), 150 mM NaCl, 1 mM EDTA (pH 8.0), 1% NP-40, 0.5% Na deoxycholate, 0.1% SDS] or SDS-Urea buffer [for the detection MLC2 and phospho-MLC2; 1% SDS, 8 mM urea, 10 mM Tris (pH 7.5), 140 mM NaCl, 5 mM EDTA, 2 mM EGTA], containing protease inhibitors and phosphatase inhibitor cocktails II and III (Roche Diagnostics) and centrifuged at 12,000 ***g*** for 10 min. Primary antibodies used were: αE-catenin (1:1000, 139700, Life Technologies), αT-catenin (1:1000, F7808, New England), N-cadherin (1:2000, 610921, BD Biosciences), β-catenin (1:1000, 712700, Life Technologies), phospho-MLC2 (1:1000, 3674, Cell Signaling), MLC2 (1:1000, 3672, Cell Signaling) and myosin IIb (1:200, M7939, Sigma). For normalization of signals, blots were also analyzed with anti-GAPDH antibody (1:5000, 6C5, RDI), followed by IRDye 680 or IRDye 800CW-conjugated secondary antibody (LI-COR). Membranes were imaged with Odyssey Infrared Imaging System (LI-COR) and quantitative densitometric analysis was performed with Odyssey version 1.2 infrared imaging software.

Preparation of subcellular fractions

Cytoplasmic and nuclear fractions were prepared using Subcellular Protein Fractionation Kit for Tissues (87790, Thermo Scientific) following the manufacturer's instructions. Briefly, P7 hearts from wild-type and DKO mice were homogenized in cytoplasmic extraction buffer with protease inhibitors. Homogenates were transferred into 15 ml tubes with Pierce tissue strainer and centrifuged at 500 ***g*** for 5 min. The supernatants were saved as cytoplasmic extract, and the pellets were re-suspended in membrane extraction buffer containing protease inhibitors and incubated at on ice for 10 min with gentle mixing. The tubes were centrifuged at 3000 ***g*** for 5 min and the supernatants were removed. Nuclear extraction buffer with $CaCl_2$ and nuclease was added to the pellets and vortexed on the highest setting for 15 s followed by incubation on ice for 30 min with gentle mixing. The tubes were centrifuged at 5000 ***g*** for 5 min and the supernatants were saved as nuclear fraction. The protein concentration was measured by BCA assay. Two hearts per sample; wild type, n=4 samples; DKO, n=3 samples.

RNA extraction and quantitative Real Time PCR

Total mRNA was isolated from hearts with TRIzol (Life Technologies) and precipitated with isopropyl alcohol. cDNA synthesis from 1 µg of total mRNA with oligo[dT]$^{12\text{-}18}$ priming and the Thermoscript RT-PCR system (Life Technologies). Quantitative reverse transcription polymerase chain reaction (qRT-PCR) was performed using the QuantStudio 5 System (Thermo Fisher Scientific) and SsoAdvanced Universal SYBR Green Supermix (Bio-Rad) according to the manufacturer's instructions. Specific primers designed for RT-PCR are listed in Table S1. For each qRT-PCR a standard curve for each gene assay was used to account for the difference of PCR efficiencies between each assay reaction. For each target gene, raw data were normalized to *Gapdh* mRNA levels.

Drug treatment

Cardiomyocytes were cultured for 4 days on glass followed by treatment for 3 or 6 h with Blebbistatin (50 µM, Calbiochem), ML-7 (50 µM, Tocris), Y27632 (20 µM, Tocris), Rho Inhibitor I (1 µg/ml, CT04, Cytoskeleton) and Rho activator II (0.5 µg/ml, CN03, Cytoskeleton) before fixation with methanol. For cardiomyocytes cultured on PA-FN hydrogels, after 4 days cells were treated for 3 h with blebbistatin, CT04 or CN03 at the indicated concentrations.

Rho GTPase activation assays

The level of RhoA-GTP in P7 hearts was measured with a RhoA G-LISA Activation Assay Kit (BK124, Cytoskeleton) following the manufacturer instructions. G-LISA Rho activation assays are ELISA-based Rho activation assays that measure the levels of GTP-bound RhoA in cells with luminometry. In brief, freshly isolated P7 hearts were homogenized in the protein extraction buffer followed by clarification by centrifugation at 9300 ***g*** at 4°C for 2 min. After determination of the protein concentration, 50 µg of the protein sample were added into the 96-well plates coated with the Rho-binding domain of Rho effector proteins and placed on an orbital shaker at 400 rpm at 4°C for 30 min. The wells were subsequently incubated at room temperature in antigen presenting buffer (Cytoskeleton) for 2 min then with anti-RhoA antibody and secondary horseradish peroxidase-conjugated antibody for 45 min at room temperature. Active RhoA levels were determined by measuring absorbance at 490 nm using a microplate spectrophotometer.

Quantification of relative β-catenin distribution in cardiomyocytes

The relative β-catenin immunosignal intensity between the longitudinal termini and the lateral membrane of individual CMs was measured using average intensity projections of a confocal image and WGA, a cell membrane marker, to demarcate the cell boundary. Images were analyzed and β-catenin signal intensity quantified using IMAGEJ 1.43 software. For each time point (n=3 hearts), the ratio of the relative β-catenin terminal/lateral signal intensity for each CM (n=60 CMs in each group) was normalized to the average β-catenin terminal/lateral ratio calculated for the 2-month-old wild-type control.

Acknowledgements

We thank Fernando Camargo for Yap floxed mice, Paola Castagnino and the ITMAT Biomechanics Core at the University of Pennsylvania for preparation of hydrogels. We are grateful to Rick Assoian, Frans van Roy and Jennifer Wilson for comments.

Competing interests

The authors declare no competing or financial interests.

Author contributions

Conceptualization: A.V., C.Z., G.L.R.; Methodology: A.V., C.Z., S.E.; Validation: A.V., C.Z.; Formal analysis: A.V., C.Z.; Investigation: A.V., C.Z., R.Y., S.E.; Writing - original draft: A.V., G.L.R.; Writing - review & editing: A.V., G.L.R.; Visualization: A.V.

Funding

This work was supported by National Institutes of Health (HL125988 to G.L.R.), by an American Heart Association Postdoctoral Fellowship (15POST22700031 to A.V.), by Grant-In-Aid (17GRNT33350088 to G.L.R.) and by the Bioimaging Core Facility of the Jefferson Kimmel Cancer Center (P30 CA056036). Deposited in PMC for release after 12 months.

Supplementary information

Supplementary information available online at
http://dev.biologists.org/lookup/doi/10.1242/dev.149823.supplemental

References

Angst, B. D., Khan, L. U. R., Severs, N. J., Whitely, K., Rothery, S., Thompson, R. P., Magee, A. I. and Gourdie, R. G. (1997). Dissociated spatial patterning of gap junctions and cell adhesion junctions during postnatal differentiation of ventricular myocardium. *Circ. Res.* **80**, 88-94.

Aragona, M., Panciera, T., Manfrin, A., Giulitti, S., Michielin, F., Elvassore, N., Dupont, S. and Piccolo, S. (2013). A mechanical checkpoint controls multicellular growth through YAP/TAZ regulation by actin-processing factors. *Cell* **154**, 1047-1059.

Berry, M. F., Engler, A. J., Woo, Y. J., Pirolli, T. J., Bish, L. T., Jayasankar, V., Morine, K. J., Gardner, T. J., Discher, D. E. and Sweeney, H. L. (2006). Mesenchymal stem cell injection after myocardial infarction improves myocardial compliance. *Am. J. Physiol. Heart Circ. Physiol.* **290**, H2196-H2203.

Chen, Q., Zhang, N., Xie, R., Wang, W., Cai, J., Choi, K.-S., David, K. K., Huang, B., Yabuta, N., Nojima, H. et al. (2015). Homeostatic control of Hippo signaling activity revealed by an endogenous activating mutation in YAP. *Genes Dev.* **29**, 1285-1297.

Chopra, A., Tabdanov, E., Patel, H., Janmey, P. A. and Kresh, J. Y. (2011). Cardiac myocyte remodeling mediated by N-cadherin-dependent mechanosensing. *Am. J. Physiol. Heart Circ. Physiol.* **300**, H1252-H1266.

Dai, X., Liu, H., Shen, S., Guo, X., Yan, H., Ji, X., Li, L., Huang, J., Feng, X.-H. and Zhao, B. (2015). YAP activates the Hippo pathway in a negative feedback loop. *Cell Res.* **25**, 1175-1178.

Das, A., Fischer, R. S., Pan, D. and Waterman, C. M. (2016). YAP nuclear localization in the absence of cell-cell contact is mediated by a filamentous actin-dependent, myosin II- and phospho-YAP-independent pathway during extracellular matrix mechanosensing. *J. Biol. Chem.* **291**, 6096-6110.

Dupont, S., Morsut, L., Aragona, M., Enzo, E., Giulitti, S., Cordenonsi, M., Zanconato, F., Le Digabel, J., Forcato, M., Bicciato, S. et al. (2011). Role of YAP/TAZ in mechanotransduction. *Nature* **474**, 179-183.

Engler, A. J., Carag-Krieger, C., Johnson, C. P., Raab, M., Tang, H.-Y., Speicher, D. W., Sanger, J. W., Sanger, J. M. and Discher, D. E. (2008). Embryonic cardiomyocytes beat best on a matrix with heart-like elasticity: scar-like rigidity inhibits beating. *J. Cell Sci.* **121**, 3794-3802.

Franke, W. W., Borrmann, C. M., Grund, C. and Pieperhoff, S. (2006). The area composita of adhering junctions connecting heart muscle cells of vertebrates. I. Molecular definition in intercalated disks of cardiomyocytes by immunoelectron microscopy of desmosomal proteins. *Eur. J. Cell Biol.* **85**, 69-82.

Goossens, S., Janssens, B., Bonne, S., De Rycke, R., Braet, F., van Hengel, J. and van Roy, F. (2007). A unique and specific interaction between alphaT-catenin and plakophilin-2 in the area composita, the mixed-type junctional structure of cardiac intercalated discs. *J. Cell Sci.* **120**, 2126-2136.

Heallen, T., Zhang, M., Wang, J., Bonilla-Claudio, M., Klysik, E., Johnson, R. L. and Martin, J. F. (2011). Hippo pathway inhibits Wnt signaling to restrain cardiomyocyte proliferation and heart size. *Science* **332**, 458-461.

Heallen, T., Morikawa, Y., Leach, J., Tao, G., Willerson, J. T., Johnson, R. L. and Martin, J. F. (2013). Hippo signaling impedes adult heart regeneration. *Development* **140**, 4683-4690.

Hirschy, A., Schatzmann, F., Ehler, E. and Perriard, J.-C. (2006). Establishment of cardiac cytoarchitecture in the developing mouse heart. *Dev. Biol.* **289**, 430-441.

Hoffman, B. D. and Yap, A. S. (2015). Towards a dynamic understanding of cadherin-based mechanobiology. *Trends Cell Biol.* **25**, 803-814.

Jacot, J. G., McCulloch, A. D. and Omens, J. H. (2008). Substrate stiffness affects the functional maturation of neonatal rat ventricular myocytes. *Biophys. J.* **95**, 3479-3487.

Janmey, P. A. and Miller, R. T. (2011). Mechanisms of mechanical signaling in development and disease. *J. Cell Sci.* **124**, 9-18.

Jopling, C., Sleep, E., Raya, M., Martí, M., Raya, A. and Izpisua Belmonte, J. C. (2010). Zebrafish heart regeneration occurs by cardiomyocyte dedifferentiation and proliferation. *Nature* **464**, 606-609.

Klein, E. A., Yin, L., Kothapalli, D., Castagnino, P., Byfield, F. J., Xu, T., Levental, I., Hawthorne, E., Janmey, P. A. and Assoian, R. K. (2009). Cell-cycle control by physiological matrix elasticity and in vivo tissue stiffening. *Curr. Biol.* **19**, 1511-1518.

Kostetskii, I., Li, J., Xiong, Y., Zhou, R., Ferrari, V. A., Patel, V. V., Molkentin, J. D. and Radice, G. L. (2005). Induced deletion of the N-cadherin gene in the heart leads to dissolution of the intercalated disc structure. *Circ. Res.* **96**, 346-354.

Leckband, D. E. and de Rooij, J. (2014). Cadherin adhesion and mechanotransduction. *Annu. Rev. Cell Dev. Biol.* **30**, 291-315.

Lecuit, T. (2010). alpha-catenin mechanosensing for adherens junctions. *Nat. Cell Biol.* **12**, 522-524.

Li, F., Wang, X., Capasso, J. M. and Gerdes, A. M. (1996). Rapid transition of cardiac myocytes from hyperplasia to hypertrophy during postnatal development. *J. Mol. Cell. Cardiol.* **28**, 1737-1746.

Li, J., Gao, E., Vite, A., Yi, R., Gomez, L., Goossens, S., van Roy, F. and Radice, G. L. (2015). Alpha-catenins control cardiomyocyte proliferation by regulating Yap activity. *Circ. Res.* **116**, 70-79.

Lin, Z., von Gise, A., Zhou, P., Gu, F., Ma, Q., Jiang, J., Yau, A. L., Buck, J. N., Gouin, K. A., van Gorp, P. R. R. et al. (2014). Cardiac-specific YAP activation improves cardiac function and survival in an experimental murine MI model. *Circ. Res.* **115**, 354-363.

Logan, C. M., Rajakaruna, S., Bowen, C., Radice, G. L., Robinson, M. L. and Menko, A. S. (2017). N-cadherin regulates signaling mechanisms required for lens fiber cell elongation and lens morphogenesis. *Dev. Biol.* **428**, 118-134.

Ma, X. and Adelstein, R. S. (2014). The role of vertebrate nonmuscle Myosin II in development and human disease. *Bioarchitecture* **4**, 88-102.

Majkut, S., Dingal, P. C. D. P. and Discher, D. E. (2014). Stress sensitivity and mechanotransduction during heart development. *Curr. Biol.* **24**, R495-R501.

Martin, A. C., Kaschube, M. and Wieschaus, E. F. (2009). Pulsed contractions of an actin-myosin network drive apical constriction. *Nature* **457**, 495-499.

Matsushita, T., Oyamada, M., Fujimoto, K., Yasuda, Y., Masuda, S., Wada, Y., Oka, T. and Takamatsu, T. (1999). Remodeling of cell-cell and cell-extracellular matrix interactions at the border zone of rat myocardial infarcts. *Circ. Res.* **85**, 1046-1055.

Mih, J. D., Sharif, A. S., Liu, F., Marinkovic, A., Symer, M. M. and Tschumperlin, D. J. (2011). A multiwell platform for studying stiffness-dependent cell biology. *PLoS ONE* **6**, e19929.

Mih, J. D., Marinkovic, A., Liu, F., Sharif, A. S. and Tschumperlin, D. J. (2012). Matrix stiffness reverses the effect of actomyosin tension on cell proliferation. *J. Cell Sci.* **125**, 5974-5983.

Miyake, Y., Inoue, N., Nishimura, K., Kinoshita, N., Hosoya, H. and Yonemura, S. (2006). Actomyosin tension is required for correct recruitment of adherens junction components and zonula occludens formation. *Exp. Cell Res.* **312**, 1637-1650.

Morikawa, Y., Zhang, M., Heallen, T., Leach, J., Tao, G., Xiao, Y., Bai, Y., Li, W., Willerson, J. T. and Martin, J. F. (2015). Actin cytoskeletal remodeling with protrusion formation is essential for heart regeneration in Hippo-deficient mice. *Sci. Signal.* **8**, ra41.

Moroishi, T., Park, H. W., Qin, B., Chen, Q., Meng, Z., Plouffe, S. W., Taniguchi, K., Yu, F.-X., Karin, M., Pan, D. et al. (2015). A YAP/TAZ-induced feedback mechanism regulates Hippo pathway homeostasis. *Genes Dev.* **29**, 1271-1284.

Paszek, M. J., Zahir, N., Johnson, K. R., Lakins, J. N., Rozenberg, G. I., Gefen, A., Reinhart-King, C. A., Margulies, S. S., Dembo, M., Boettiger, D. et al. (2005). Tensional homeostasis and the malignant phenotype. *Cancer Cell* **8**, 241-254.

Porrello, E. R., Mahmoud, A. I., Simpson, E., Hill, J. A., Richardson, J. A., Olson, E. N. and Sadek, H. A. (2011). Transient regenerative potential of the neonatal mouse heart. *Science* **331**, 1078-1080.

Porrello, E. R., Mahmoud, A. I., Simpson, E., Johnson, B. A., Grinsfelder, D., Canseco, D., Mammen, P. P., Rothermel, B. A., Olson, E. N. and Sadek, H. A. (2013). Regulation of neonatal and adult mammalian heart regeneration by the miR-15 family. *Proc. Natl. Acad. Sci. USA* **110**, 187-192.

Poss, K. D., Wilson, L. G. and Keating, M. T. (2002). Heart regeneration in zebrafish. *Science* **298**, 2188-2190.

Rauzi, M., Lenne, P.-F. and Lecuit, T. (2010). Planar polarized actomyosin contractile flows control epithelial junction remodelling. *Nature* **468**, 1110-1114.

Schlegelmilch, K., Mohseni, M., Kirak, O., Pruszak, J., Rodriguez, J. R., Zhou, D., Kreger, B. T., Vasioukhin, V., Avruch, J., Brummelkamp, T. R. et al. (2011). Yap1 acts downstream of alpha-catenin to control epidermal proliferation. *Cell* **144**, 782-795.

Shewan, A. M., Maddugoda, M., Kraemer, A., Stehbens, S. J., Verma, S., Kovacs, E. M. and Yap, A. S. (2005). Myosin 2 is a key Rho kinase target necessary for the local concentration of E-cadherin at cell-cell contacts. *Mol. Biol. Cell* **16**, 4531-4542.

Smutny, M., Cox, H. L., Leerberg, J. M., Kovacs, E. M., Conti, M. A., Ferguson, C., Hamilton, N. A., Parton, R. G., Adelstein, R. S. and Yap, A. S. (2010). Myosin II isoforms identify distinct functional modules that support integrity of the epithelial zonula adherens. *Nat. Cell Biol.* **12**, 696-702.

Soonpaa, M. H., Kim, K. K., Pajak, L., Franklin, M. and Field, L. J. (1996). Cardiomyocyte DNA synthesis and binucleation during murine development. *Am. J. Physiol.* **271**, H2183-H2189.

Swope, D., Cheng, L., Gao, E., Li, J. and Radice, G. L. (2012). Loss of cadherin-binding proteins beta-catenin and plakoglobin in the heart leads to gap junction remodeling and arrhythmogenesis. *Mol. Cell. Biol.* **32**, 1056-1067.

Takeda, K., Kishi, H., Ma, X., Yu, Z. X. and Adelstein, R. S. (2003). Ablation and mutation of nonmuscle myosin heavy chain II-B results in a defect in cardiac myocyte cytokinesis. *Circ. Res.* **93**, 330-337.

von Gise, A., Lin, Z., Schlegelmilch, K., Honor, L. B., Pan, G. M., Buck, J. N., Ma, Q., Ishiwata, T., Zhou, B., Camargo, F. D. et al. (2012). YAP1, the nuclear target of Hippo signaling, stimulates heart growth through cardiomyocyte proliferation but not hypertrophy. *Proc. Natl. Acad. Sci. USA* **109**, 2394-2399.

Wada, K.-I., Itoga, K., Okano, T., Yonemura, S. and Sasaki, H. (2011). Hippo pathway regulation by cell morphology and stress fibers. *Development* **138**, 3907-3914.

Wang, H.-B., Dembo, M. and Wang, Y.-L. (2000). Substrate flexibility regulates growth and apoptosis of normal but not transformed cells. *Am. J. Physiol. Cell Physiol.* **279**, C1345-C1350.

Wei, L., Imanaka-Yoshida, K., Wang, L., Zhan, S., Schneider, M. D., DeMayo, F. J. and Schwartz, R. J. (2002). Inhibition of Rho family GTPases by Rho GDP

dissociation inhibitor disrupts cardiac morphogenesis and inhibits cardiomyocyte proliferation. *Development* **129**, 1705-1714.

Wickline, E. D., Dale, I. W., Merkel, C. D., Heier, J. A., Stolz, D. B. and Kwiatkowski, A. V. (2016). alphaT-catenin is a constitutive actin-binding alpha-catenin that directly couples the cadherin catenin complex to actin filaments. *J. Biol. Chem.* **291**, 15687-15699.

Xin, M., Kim, Y., Sutherland, L. B., Qi, X., McAnally, J., Schwartz, R. J., Richardson, J. A., Bassel-Duby, R. and Olson, E. N. (2011). Regulation of insulin-like growth factor signaling by Yap governs cardiomyocyte proliferation and embryonic heart size. *Sci. Signal.* **4**, ra70.

Xin, M., Kim, Y., Sutherland, L. B., Murakami, M., Qi, X., McAnally, J., Porrello, E. R., Mahmoud, A. I., Tan, W., Shelton, J. M. et al. (2013). Hippo pathway effector Yap promotes cardiac regeneration. *Proc. Natl. Acad. Sci. USA* **110**, 13839-13844.

Yahalom-Ronen, Y., Rajchman, D., Sarig, R., Geiger, B. and Tzahor, E. (2015). Reduced matrix rigidity promotes neonatal cardiomyocyte dedifferentiation, proliferation and clonal expansion. *eLife* **4**, e07455.

Yao, M., Qiu, W., Liu, R., Efremov, A. K., Cong, P., Seddiki, R., Payre, M., Lim, C. T., Ladoux, B., Mege, R.-M. et al. (2014). Force-dependent conformational switch of alpha-catenin controls vinculin binding. *Nat. Commun.* **5**, 4525.

Yonemura, S., Wada, Y., Watanabe, T., Nagafuchi, A. and Shibata, M. (2010). alpha-Catenin as a tension transducer that induces adherens junction development. *Nat. Cell Biol.* **12**, 533-542.

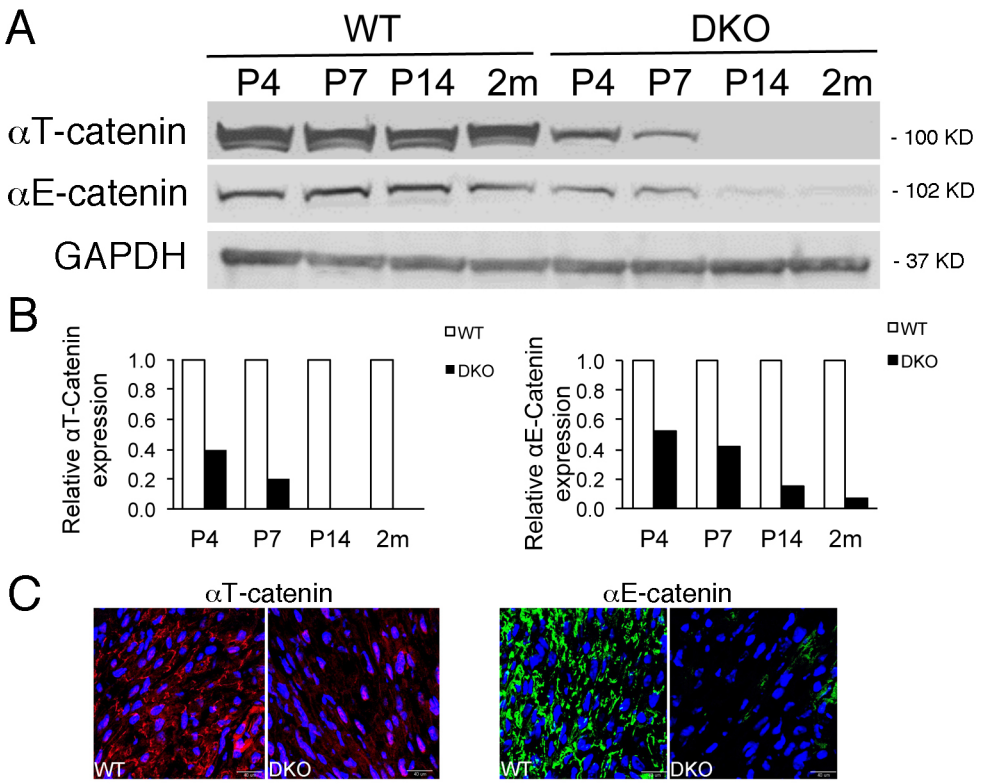

Supplementary Figure 1

Supplementary Figure 1. Loss of αT- and αE-catenins in DKO hearts. (A) Representative image of Western blot analysis of heart lysates from P4, P7, P14 and 2-month-old WT and DKO mice and (B) quantification of αT- and αE-catenin expression relative to WT, n=4 individual hearts/time point. (C) Representative immunofluorescent images of heart sections from P4 WT and DKO mice. Sections were stained for αT-catenin (red) and (B) αE-catenin (green).

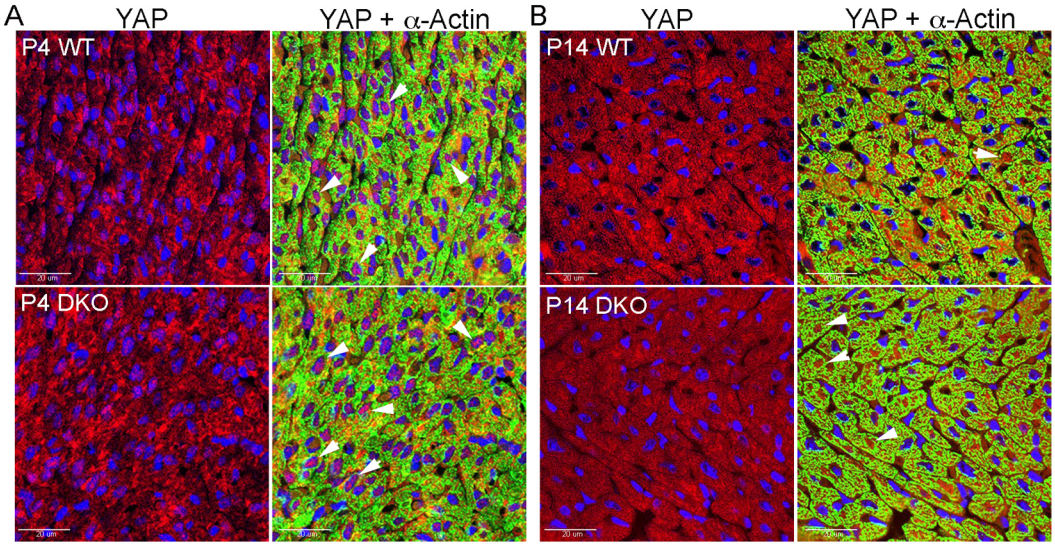

Supplementary Figure 2

Supplementary Figure 2. Yap expression in postnatal hearts. Representative immunofluorescent images of heart sections from (A) P4 and (B) P14 WT and DKO mice. Sections were co-stained for Yap (red) and α-Actin (green). Note the decrease in nuclear Yap-positive cardiomyocytes between P4 and P14 (arrowheads).

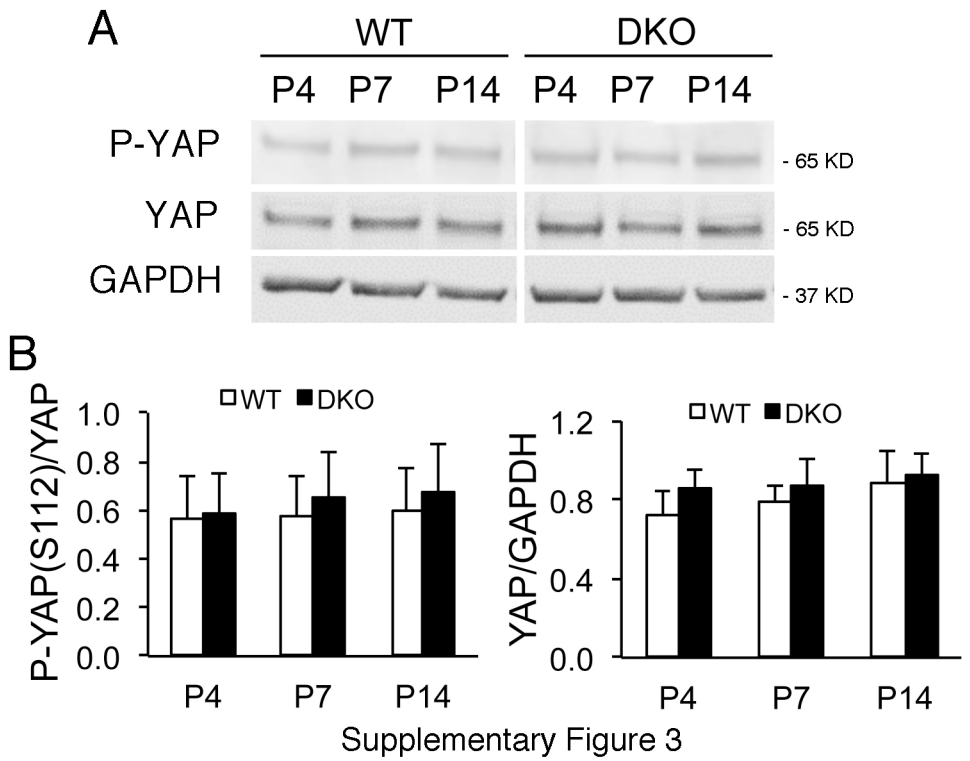

Supplementary Figure 3. Western analysis of Yap in postnatal hearts. (A) Representative image of Western blot analysis of heart lysates from P4, P7, and P14 WT and DKO mice and (B) quantification of phosphorylated (p) Yap at serine 112 and total Yap levels, n=4 individual hearts/time point. NS, by Student's *t*-test. Error bars represent s.e.m..

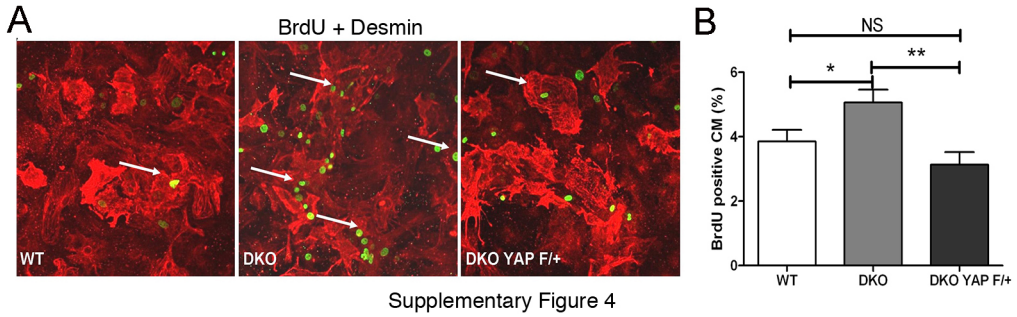

Supplementary Figure 4

Supplementary Figure 4. Increase proliferation in cultured α-catenin DKO cardiomyocytes. (A) Representative images of BrdU (5-Bromo-2'-deoxyuridine, green) incorporation (arrows) in cultured neonatal cardiomyocytes. Cells were co-stained for the cardiac marker desmin (red). (B) Quantification of BrdU-positive cardiomyocytes from WT, DKO and DKO Yap +/- mice. *, p <0.05, **, p<0.01 by Student's *t*-test. Error bars represent s.e.m..

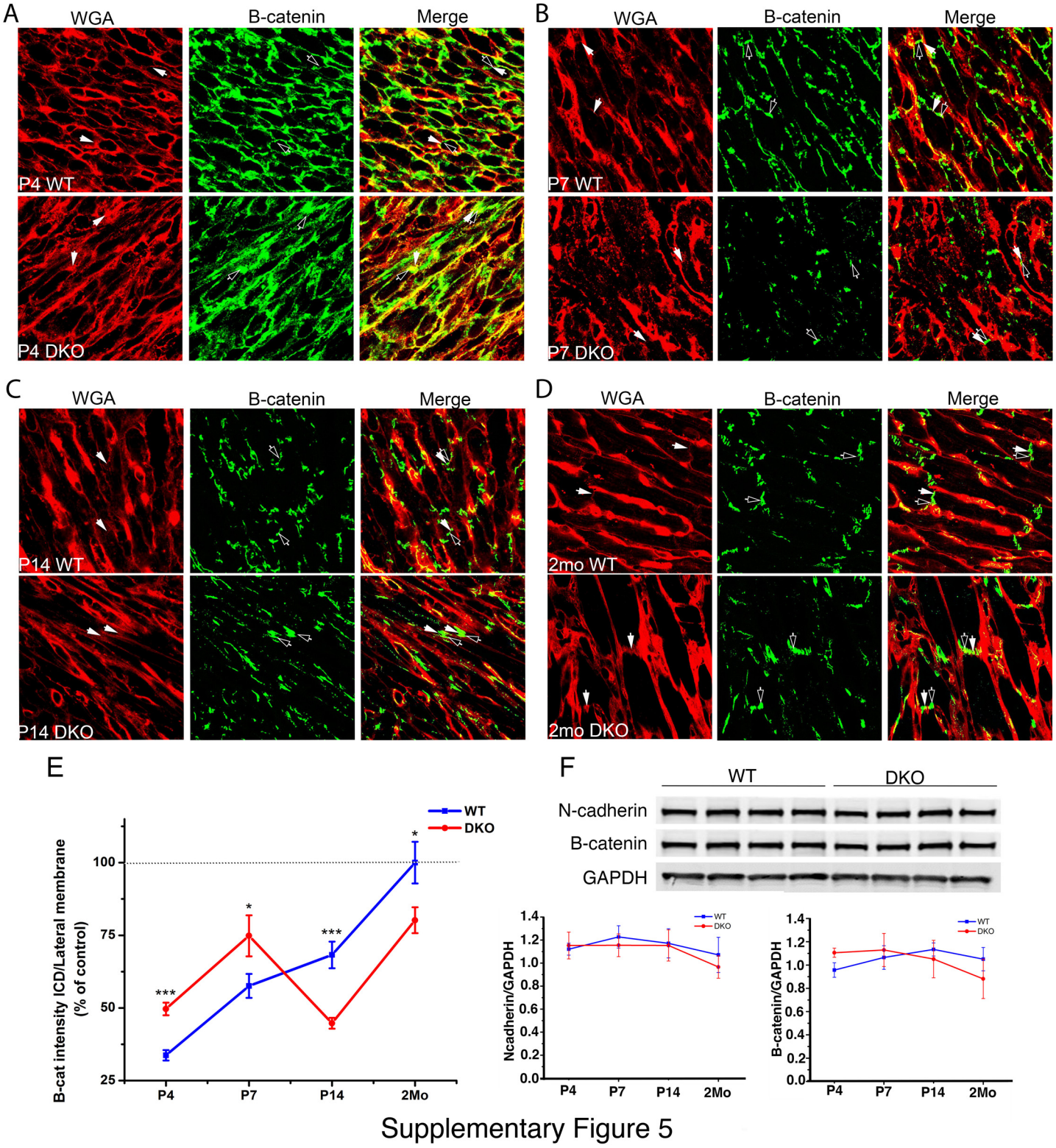

Supplementary Figure 5

Supplementary Figure 5. Analysis of β-catenin cellular distribution in cardiomyocytes during postnatal heart development. Representative immunofluorescent images of heart sections from (A) P4, (B) P7, (C) P14, and (D) 2-month-old WT and DKO mice. Sections were co-stained for β-catenin (green, hollow arrowheads) and WGA (red, solid arrowheads). (E) For each time point (N=3 hearts), the ratio of the relative β-catenin terminal/lateral signal intensity for each CM (n=60 CMs in each group) was normalized to the average β-catenin terminal/lateral ratio calculated for the 2 month WT control. (F) Western analysis of N-cadherin and β-catenin heart lysates from P4, P7, P14 and 2-month-old WT and DKO mice. n=4 individual hearts/time point. *, $p < 0.05$, ***, $p > 0.001$ by Student's *t*-test. Error bars represent s.e.m..

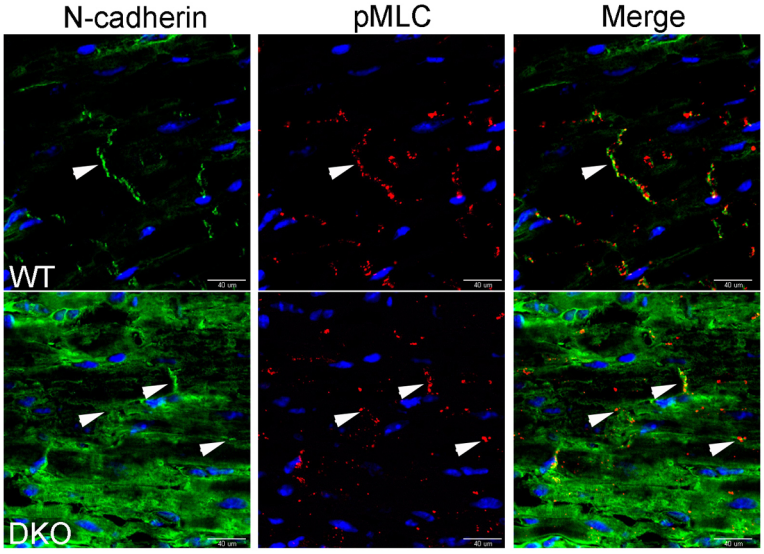

Supplementary Figure 6. Mislocalization of actomyosin activity in adult α-catenin DKO hearts.

Representative immunofluorescent images of heart sections from 2-month-old WT and DKO mice. Sections were co-stained for N-cadherin (green, arrowheads) and pMLC (red, arrowheads).

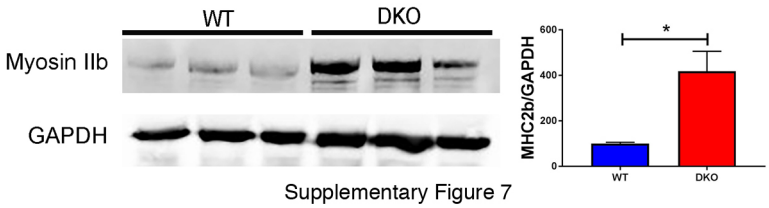

Supplementary Figure 7. Myosin IIb expression in adult hearts. Western blot analysis and quantification of Myosin IIb expression in whole heart lysates from 2-month-old WT and DKO mice. *, $p < 0.05$ by Student's *t*-test. Error bars represent s.e.m..

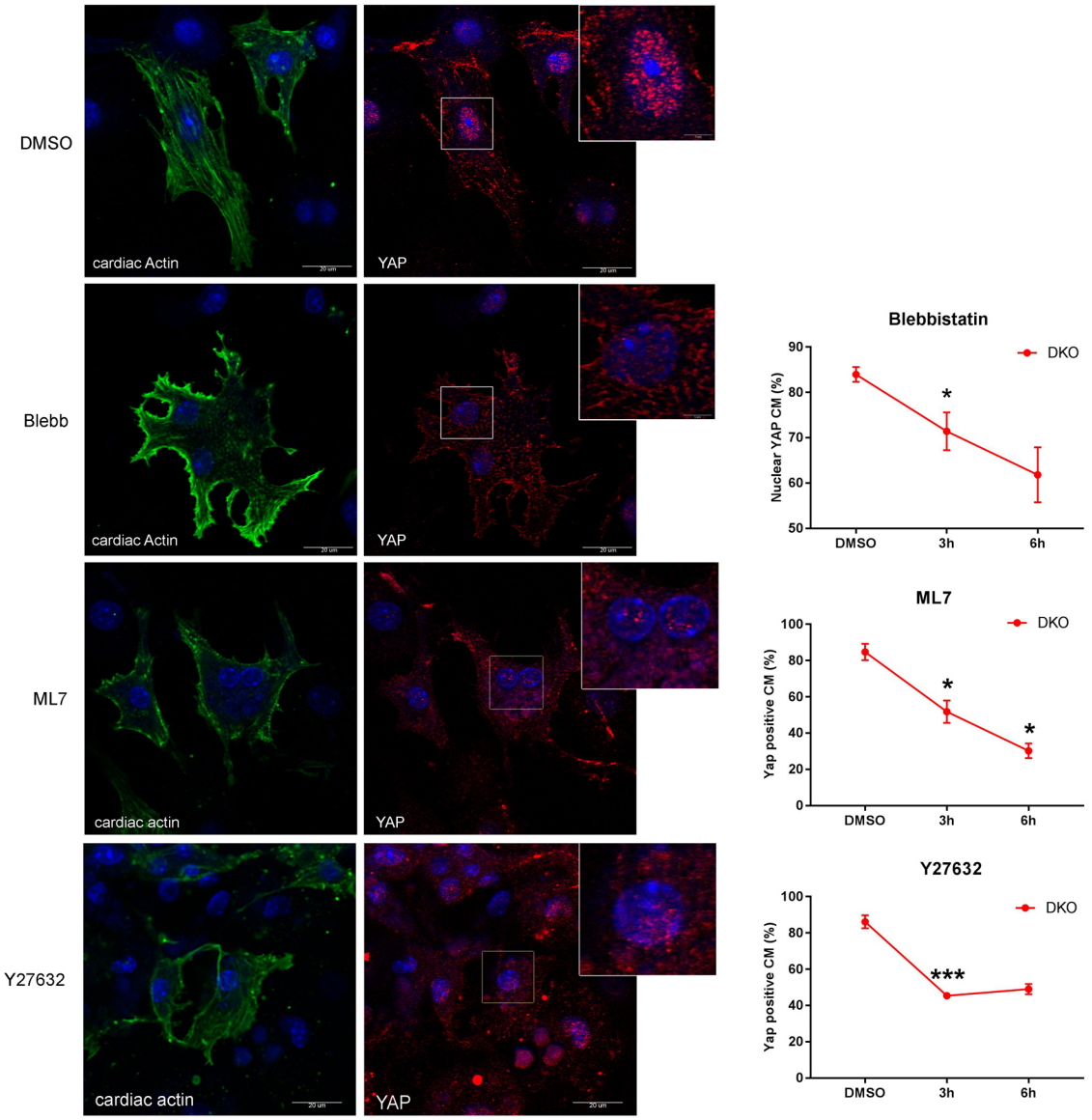

Supplementary Figure 8

Supplementary Figure 8. Inhibition of ROCK/MLCK pathway in α-catenin DKO cardiomyocytes causes Yap to exit the nucleus. Representatives images of DKO cardiomyocytes cultured on glass for 4 days and treated for 3 hr (shown) or 6 hr with Blebbistatin (50 μM), Myosin Light Chain Kinase (MLCK) inhibitor ML7 (20 μM) or Rho-associated protein kinase (ROCK) inhibitor Y27632 (20 μM). The cells were co-stained for Yap (red) and α-actin (green). Right, quantification of nuclear Yap-positive cardiomyocytes after Blebblistatin, ML7 or Y27632 for 3 or 6 hr (N=3 experiments, n= minimum 100 cells/experiment). *, $p < 0.05$, ***, $p < 0.001$ by Student's *t*-test. Error bars represent s.e.m..

Supplementary Table I: Primers used for qRT-PCR

mGAPGH F	CATCTTCCAGGAGCGAGACC
mGAPGH R	CTCGTGGTTCACACCCATCA
mSGCD F	GACTCTCATCCGCCACTCTG
mSGCD R	AGGCATCTTTTCCTCCAGCC
mCTGF F	GAACAAATGCTGTGCAGGTGA
mCTGF R	TCCTGGTAGGAATCGGACCTT
mCYR61 F	CTGCGCTAAACAACTCAACGA
mCYR61 R	GCAGATCCCTTTCAGAGCGG
mBIRC5 F	CAGATCTGGCAGCTGTACCT
mBIRC5 R	CTCCGCCATTCGCTCTGG
mLIN9 F	GAAATCCCTCTACCCCTGGTT
mLIN9 R	GTGTCCACTGCATCTATCTGAC
mAURKb F	CAGAAGGAGAACGCCTACCC
mAURKb R	GAGAGCAAGCGCAGATGTC